A portable N-terminal biphenyl motif in LL-37 enhances the activity of short human cathelicidin derivatives

John S. Albin[1,2,3*], Dimuthu A. Vithanage[2,3], Corey Johnson[2,3], and Bradley L. Pentelute[1,4-6]

[1]Department of Chemistry, Massachusetts Institute of Technology, Cambridge, MA, 02139, USA

[2]Division of Infectious Diseases, Massachusetts General Hospital, Boston, MA, 02114, USA

[3]Harvard Medical School, Boston, MA, 02115, USA

[4]The Koch Institute for Integrative Cancer Research, Massachusetts Institute of Technology, Cambridge, MA 02142, USA

[5]Center for Environmental Health Sciences, Massachusetts Institute of Technology, Cambridge, MA 02139, USA

[6]Broad Institute of MIT and Harvard, Cambridge, MA 02142, USA

*Correspondence: jalbin@mgh.harvard.edu

Summary: Issues such as potency and stability limit our ability to realize the potential of host defense peptides (HDPs) to serve as new antibiotics. Informed by our prior structure-activity work, we demonstrate that transposition of an N-terminal biphenyl motif from full-length LL-37 onto the previously-described central activity region (residues 18-29) improves activity against gram-negative bacteria by >16-fold. We further improve upon this lead derivative, termed FF-14, using stabilizing modifications such as D-amino acids and C-terminal amidation as well as selected N-lipidation moieties, and demonstrate the transferability of biphenyl motif activity to longer cathelicidin scaffolds. Mechanistic interrogation reveals that the biphenyl pharmacophore increases both inner and outer membrane permeabilization, though with effect sizes suggestive of additional mechanisms of gram-negative killing. Inclusion of the LL-37 biphenyl motif is thus a portable strategy for augmenting short cathelicidin activity and better approximating the activity profile of LL-37 itself in short sequences.

Keywords: LL-37, cathelicidin, antimicrobial peptide, host defense peptide, Escherichia coli, Pseudomonas aeruginosa, antibiotic, peptide, peptidomimetic, membrane permeabilization

Introduction

Antimicrobial resistance is a growing threat to human health, accounting for 1.2 million deaths in 2019, particularly due to infections with resistant gram-negative bacteria[1]. Absent the development of new antibiotics, this death toll is expected to escalate in the coming decades[2]. One approach to the pursuit of new antibiotics is to develop derivatives of host defense peptides (HDPs), which are structurally diverse peptides produced by all branches of life to defend against microbes[3,4]. Human HDPs, in particular, are attractive templates. Having evolved in the context of the human immune system, LL-37 and other human HDP templates are generally nonimmunogenic in their starting sequences, but may encode desirable immunomodulatory activities to enhance the clearance of an infection[5–8]. Moreover, because these templates are chemically simple, it is straightforward to diversify their structures through the application of noncanonical amino acids and combinatorial chemistry[9].

Despite their promise, the clinical impact of HDPs has been limited by familiar issues such as stability, pharmacokinetics, toxicity, and potency[10]. Though significant, these barriers also present clear opportunities to apply well-characterized peptide-engineering strategies. Consider GLP-1 agonists, for example. Native GLP-1(7-37) is a short, helical peptide with poor stability and pharmacokinetics. The difference between this nonviable therapeutic lead and the transformative drug semaglutide is three amino acid changes aimed primarily at improving the stability and pharmacokinetics of the native peptide[11]. In principle, the same rules should apply to structurally similar helical peptides such as LL-37, which is active against gram-negative bacteria and demonstrates a wide range of proposed immunomodulatory functions that may be of therapeutic utility[12–18].

There are a number of well-characterized approaches by which to modulate peptide stability through strategies such as stapling[19,20], primary sequence changes[11], and peptidomimetic alterations including the use of D-amino acids inert to native L-proteases[21]. Many of these have been directly applied to cathelicidin derivatives before, and it is likely that

they will prove relevant to many distinct primary cathelicidin sequences. Similarly, it is probable that the same lipidation strategies that can improve peptide pharmacokinetic properties in endocrinology will also prove useful with cathelicidin derivatives[22].

Less obvious, however, is the path forward for addressing issues of cathelicidin toxicity and antimicrobial potency, which pose barriers beyond those common to endocrine peptides. Many prior reports describe the activities of diverse fragments of LL-37[23], for example, but it is not always clear to what extent these short units remain structurally stable and mechanistically analogous to LL-37 – or why. A further limiting factor is the incomplete selectivity of cathelicidin derivatives between mammalian and bacterial membranes, which can be difficult to ablate even in highly optimized HDP sequences[24,25]. To address this toxicity gap, we have recently reported structure-activity relationships in full-length LL-37 that revealed a rational approach to separating activity against gram-negative and mammalian cell membranes by limiting cathelicidin oligomerization[26,27].

The study presented here builds on a separate observation from these structure-activity relationship studies, namely the loss of antimicrobial activity among some mutants with changes predominantly in the LL-37 N-terminus. This loss of activity with mutations linearly distant from the core activity region spanning residues 18-29 suggests that N-terminal residues may be important for the recapitulation of native LL-37-like activity against gram-negative bacteria[28,29].

Developing this hypothesis, we report here that transposition of an N-terminal biphenyl motif to the previously described core activity region yields an enhanced short cathelicidin derivative, FF-14, with >16-fold improved potency against gram-negative bacteria compared with the core activity region alone. We further find that common stabilization strategies such as the use of D-amino acids and C-terminal amidation remain applicable in this template, and that selected N-lipidation moieties may also help to limit mammalian cell toxicity. Mechanistic interrogation reveals that gram-negative outer and inner membrane permeabilization increases with each sequential addition of Phe to the N-terminus, with permeabilization by FF-14

approximating that of LL-37. The studies described here thus highlight the importance and portability of the biphenyl motif for antimicrobial activity among human cathelicidin derivatives while laying the groundwork for integration with additional strategies for the rational detoxification and pharmacokinetic control of cathelicidin antimicrobials.

Results

Limited activity of short derivatives of LL-37 against gram-negative bacteria

By convention, peptide derivatives of the human cathelicidin *CAMP* gene are named according to their first two amino acids and their overall length – thus, LL-37 starts with the amino acids Leu-Leu and is 37 residues long[30–33]. A large number of studies have previously reported on the activity of distinct fragments of LL-37[23]. Among these, KR-12, a 12-residue fragment extending from residues 18-29 of the native LL-37 peptide, is generally considered the definitive minimal unit of LL-37 activity to which many peptidomimetic alterations have been previously applied[28,34–45].

The initial description of KR-12 suggests only modest potency, with a minimum inhibitory concentration (MIC) of 40 μM against *Escherichia coli* K12, which in those studies was equivalent to the MICs seen with another derivative, FK-13[46,47], as well as wild-type LL-37. A follow-up study revealed similarly modest antimicrobial activity of KR-12 itself at >50 μM against *E. coli* (identical to our findings below)[45], though results can vary with the methods used for susceptibility testing[42,45]. By contrast, most approved antibiotics active against *Enterobacterales* have Clinical & Laboratory Standards Institute (CLSI) minimum inhibitory concentration (MIC) cutoffs in the single-digit micromolar range[48]. Thus, although KR-12 is the shortest unit of LL-37 activity, the overall potency of this primary sequence is somewhat lower than is likely to be required in order to eventually derive clinically useful antimicrobials from LL-37 templates. Even FK-13, which is slightly more potent than KR-12 in most studies but still relatively non-toxic, is borderline by this measure[49]. We therefore sought to identify short derivatives of LL-37 with greater potency, from which we might then apply structure-activity approaches such as those that we have used to detoxify full-length LL-37 while conserving antimicrobial activity[29].

To revisit the subject of shorter LL-37 derivatives comparable in size to approved antimicrobial natural products such as daptomycin and colistin, we made a series of fragments of LL-37 based on prior studies and assessed their relative activity against *E. coli* and

Pseudomonas aeruginosa as well as their hemolytic activity against defibrinated sheep blood, where we take hemolysis as an *in vitro* surrogate of activity against mammalian cell membranes. Among these fragments, all except LL-25, GD-23, FK-13, and full-length LL-37 demonstrated MICs > 50 μM against *E. coli*, indicative of generally low levels of antimicrobial activity (**Figure 1A**). Similar results were seen with *P. aeruginosa* in **Figure 1B**. Consistent with their low levels of antimicrobial activity, most derivatives demonstrated little to no hemolytic activity in **Figure 1C**, the major exception being control wild-type LL-37. An alignment of these initial derivatives is shown in **Figure 1D**.

Thus, while many LL-37 derivatives show low toxicity to mammalian cell membranes, these generally also lack potent activity against gram-negative bacteria, limiting their utility as starting points for the development of new antibiotics based on the LL-37 scaffold. The major exceptions to this rule are LL-25 and GD-23, each of which recapitulates the separation of hemolytic and antimicrobial activities that we have observed separately in selected mutants of full-length LL-37. This may reflect the absence of residues that we have previously found to be important both for oligomerization and for global membrane permeabilization activity, though further exploration of this theme is beyond the scope of the present studies (see also **Discussion**)[29]. **Figure S1** provides a histogram depiction of the data in **Figure 1** including error bars. **Figures S2-14** (antimicrobial susceptibility) and **15-27** (hemolysis) show the kinetic growth and hemolysis curves associated with each experimental endpoint depicted in **Figure 1**. **Table S1** provides a standard, quantitative summary of the results in **Figure 1**.

Mimicry of the LL-37 N-terminus improves the activity of short derivatives of LL-37 against gram-negative bacteria

Among the peptides in **Figure 1**, we noted that the most active candidates tended to include greater proportions of the LL-37 N-terminus. This is consistent with structure-activity mutagenesis that we have recently reported in full-length LL-37, in which grouped Ala

mutagenesis of the LL-37 N-terminus ablates LL-37 activity against gram-negative bacteria despite being distant in linear sequence from the putative core activity region surrounding LL-37 residues 18-29[29]. One of these surface mutagenesis derivatives, in particular, has no mutations within the core activity region, but is notable for containing two of the four Phe residues in LL-37 as a biphenyl motif. In wild-type LL-37, these four native Phe residues are thought to be primary mediators of membrane interaction, and conserved aromatic residues are also found among α defensins[28,50]. Finally, we noted that the inclusion of N-terminal Phe in FK-13 yielded improved activity over the KR-12 minimal unit (**Figure 1**). We therefore reasoned that transposition of the LL-37 N-terminal biphenyl motif, FF[RK], to the N-terminus of KR-12, [KR], might yield a short derivative of LL-37 with improved antimicrobial activity.

To test this hypothesis, we made derivatives FF-14 and FF-14-RK, in which the N-terminal biphenyl motif of LL-37 was transposed onto the central 18-29 (KR-12) region. As shown in **Figures 2A-B**, this results in 14-mer derivatives of LL-37 that more closely mimic the antimicrobial activities of wild-type LL-37, including potency >16-times greater than KR-12 (3.1 μM for FF-14 versus >50 μM for KR-12 against *E. coli*) and 4-times greater than FK-13, safely into low micromolar MIC ranges closer to those of many approved antibiotics. Although this comes at a cost of increased hemolysis relative to KR-12 / FK-13, hemolysis among these 14-mers remained 4-8 times less than LL-37 (**Figure 2C**); no substantial differences were noted based on the ordering of [KR] within this motif.

Mimicry of an LL-37 N-terminal sequence motif within FF-14 thus yields a scaffold with >16-fold improvements in activity, thus providing the basis for further modification of this scaffold toward the development of cathelicidin-derived antibiotics. The sequences of these and other derivatives tested are shown in **Figure 2D**.

D-amino acids and C-terminal amidation improve FF-14 activity against gram-negative bacteria

A number of peptidomimetic alterations have been demonstrated to stabilize and improve upon the native activities of HDP scaffolds such as D-amino acids and end modifications (*e.g.* [35,46,51,52] among examples with LL-37 and derivatives thereof). To determine whether similar alterations would prove compatible with FF-14, we made an expanded set of peptidomimetic derivatives in which FF-14 was either changed to an all-D configuration or amidated at the C-terminus. As shown in **Figure 2A-B**, enantiomeric ff-14 and C-amidated FF-14 each demonstrated similar-to-improved antimicrobial activity, particularly against *E. coli*, with similar shifts in fold-separation between the 20% hemolysis threshold and MIC (**Table S2**). Synthetic leads based on the FF-14 template may therefore benefit from the inclusion of stabilizing mutations such as the incorporation of D-amino acids and C-terminal amidation. Of note, activity of FK-13 also improved in the all-D format, with retention of the same fold-separation between its 20% hemolysis threshold and MIC. Although retro-inverso fk-13 also retained activity equivalent to all-D fk-13, retro-FK-13 lost all apparent antimicrobial activity.

Thus, FF-14 is compatible with standard stabilization approaches such as D-amino acids and C-amidation. **Figure S28** provides a histogram depiction of the data in **Figure 2** including error bars. **Figures S29-41** (antimicrobial susceptibility) and **42-54** (hemolysis) show the kinetic growth and hemolysis curves associated with each experimental endpoint depicted in **Figure 2**. **Table S2** provides a standard, quantitative summary of the results in **Figure 2**.

Perfluoroaryl stapling does not reliably separate antimicrobial and hemolytic cathelicidin activities

Despite the improved activity of FF-14 and derivatives thereof against gram-negative bacteria, we noted substantial ongoing hemolytic activity that would likely preclude the use of these cathelicidin derivatives as lead therapeutics without additional detoxifying modifications. In related work, we have previously identified I24 and L28 as the primary determinants of mammalian cell toxicity in full-length LL-37[29]. Consistent with this finding, LL-25 and GD-23 in

Figure 1 omit L28 and demonstrate decreased hemolytic activity. Moreover, in separate mutagenesis of the FF-14 template, we have found that substitution of the I24 equivalent residue with aminoisobutyric acid (Aib) may contribute to diminished hemolytic activity[26]. Because equivalents of I24 and L28 occur within the KR-12 core (I9 and L13 in FF-14 numbering), we hypothesized that stapling strategies, particularly those involving I9 and L13, might result in similar ablation of toxicity within FF-14 while preserving antimicrobial activity.

To test this hypothesis, we made a comprehensive set of *i*,*i*+3, *i*,*i*+4, and *i*,*i*+7 perfluoroaryl stapled versions of the FF-14 hydrophobic surface as well as selected perfluoroaryl stapled versions of FK-13[19]. The general scheme for stapling at Cys residues under this methodology is shown in **Figure 3**. As shown in **Figures 4A-B**, perfluoroaryl stapling of FK-13 and FF-14 derivatives generally proved neutral-to-detrimental to overall antimicrobial activity, and in most cases failed to substantially improve upon the characteristics of the associated primary sequence alone. Pilot experiments with lactam and Pd arylation stapling chemistries did not improve upon these results (data not shown). We further noted the tendency of most staples to carry hydrophobic properties comparable to our perfluoroaryl moieties, which may contribute to ongoing hemolysis. Although one prior study of *i*,*i*+4 and *i*,*i*+7 hydrocarbon stapled KR-12 derivatives found some benefit of stapling in the less active KR-12 template, we did not generally observe added value with the more active FF-14 primary sequence[39].

In summary, although stapling might prove useful in the context of primary sequences with lower intrinsic activity, or perhaps when using chemistries with more hydrophilic character, our data favor changes in primary sequence as a more productive approach to modulating cathelicidin toxicity[26,29]. **Figure S55** provides a histogram depiction of the data in **Figure 4** including error bars. **Figures S56-70** (antimicrobial susceptibility) and **71-85** (hemolysis) show the kinetic growth and hemolysis curves associated with each experimental endpoint depicted in **Figure 4**. **Table S3** provides a standard, quantitative summary of the results in **Figure 4**.

N-lipidation modulates FF-14 activity

A lipid tail is important for the activity of certain antibiotics such as colistin and daptomycin. Along these lines, prior studies have indicated that some lipid tails can improve the activity of the KR-12 template[45,53,54], though often at a cost of toxicity. Moreover, the potential impact of N-lipidation is implied by the hydrophobic character of the LL-37 N-terminus, where two Leu residues precede the native biphenyl motif – L_1LGDFF_6. We therefore reasoned that N-lipidation might also affect the activity of FF-14 or FK-13 and proceeded to test the effects of lipid moieties of several structural types on the antimicrobial and hemolytic activities in FF-14, with an emphasis on lipid moieties found in approved antimicrobials (*e.g.*, 5-dimethylamino pentanoic acid, 10-methylundecanoic acid, and chlorobiphenyl in lipoglycopeptides) or in promising experimental scaffolds such as biphenyl moieties[55]. Of note, these are largely distinct from those previously reported in the context of KR-12[45,53,54]. Moieties used in **Figures 6** or **7** are shown in **Figure 5**; **Figure S86** shows additional moieties tested in the context of FK-13 in **Figure S87**.

As shown in **Figures 6A-B**, the addition of several moieties to the FF-14 N-terminus results in improved antimicrobial activity, though only 5-dimethylamino-pentanoic acid yielded neutral-to-improved potency by halving the FF-14 MIC while maintaining the same 20% toxicity threshold (**Table S4**). Despite its activity in *E. coli*, this and most derivatives demonstrated diminished activity against *P. aeruginosa*. Additional lipid tails were tested in the context of FK-13, though again typically with a directional correlation between antimicrobial activity and hemolytic activity (**Figures S86-87**).

Figure 6 thus shows that the additive value of N-lipidation within the FF-14 template is largely limited to 5-dimethylamino pentanoic acid, though future work on placement elsewhere within cathelicidin templates may prove fruitful. In particular, appending further phenyl groups to the N-terminus beyond the biphenyl motif itself as in 4-Cl-Bph did not yield additional increases in activity. As in the case of stapling, our data support the principle that the most efficient route

to improved cathelicidin sequences runs through primary sequence modifications. **Figure S88-89** provides a histogram depiction of the data in **Figure 6** and **Figure S87**, including error bars. **Figures S90-105** (antimicrobial susceptibility) and **106-121** (hemolysis) show the kinetic growth and hemolysis curves associated with each experimental endpoint depicted in **Figure 6** and **Figure S87**. **Table S4** provides a standard, quantitative summary of the results in **Figure 6**. **Table S5** provides a standard, quantitative summary of the results in **Figure S87**.

Placement of a biphenyl motif to recapitulate FF-14 within longer cathelicidin-derived sequences improves antimicrobial activity

Based on the results in **Figure 6** and **Figure S87**, we elected to further examine three candidate N-lipidation moieties – octanoic acid (Oct), 5-dimethylamino pentanoic acid (DMA), and the quaternary amine equivalent of DMA, δ valerobetaine (DVB). We further expanded the application of these moieties to the longer cathelicidin derivatives LL-25 and GD-23 noted in **Figure 1** that partially separate antimicrobial and hemolytic activity. Finally, to test the impact of recapitulating the FF-14 sequence within these longer cathelicidin scaffolds, we included derivatives of LL-25 and GD-23 with duplicate biphenyl motifs – the native sequence at the N-terminus, and the FF-14 sequence within the central activity region.

As shown in **Figure 7** and quantitated in **Table S6**, most N-lipidated derivatives of LL-25 and GD-23 demonstrated diminished antimicrobial activity compared to the wild-type primary sequence. Activity of N-lipidated derivatives against *P. aeruginosa* was entirely ablated for these sequences in the case of DMA and DVB. Oct-GD-23 demonstrated improved antimicrobial activity, though at some cost of hemolytic activity. Consistent with the effects of DMA in **Figure 6**, however, DVB did yield four-fold separation between antimicrobial and hemolytic activity in the context of FF-14. Among the modifications tested, however, the greatest impact on antimicrobial activity was observed when including a second biphenyl motif to recapitulate the FF-14 sequence within the longer LL-25 and GD-23 scaffolds. This was particularly true for

activity against *P. aeruginosa*, where inclusion of this second biphenyl motif to recapitulate the FF-14 sequence improved MICs from 25 to 6.3 for LL-25 and from >50 to 12.5 for GD-23.

With the possible exceptions of DMA or DVB in the context of shorter derivatives such as FF-14, lipidation generally did not improve upon the characteristics of the native sequence in derivatives LL-25 and GD-23. Duplication of the biphenyl motif to recapitulate FF-14 within the longer scaffolds LL-25 and GD-23, however, did improve antimicrobial activity, particularly against *P. aeruginosa*. Placement of the biphenyl pharmacophore within LL-25, for example, decreases the MIC against *P. aeruginosa* 4-fold from 25 μM to 6.3 μM.

Thus, the biphenyl motif is portable also to longer cathelicidin scaffolds beyond FF-14. Moreover, our results again demonstrate that for cathelicidin templates that are already highly active, the expected contributions of peptidomimetic modifications to the primary sequence itself are generally marginal. Efforts to modulate cathelicidin antimicrobial activity and toxicity may more efficiently address these goals by focusing on primary sequence modifications.

Figure S122 provides a histogram depiction of the data in **Figure 7**, including error bars. **Figures S123-136** (antimicrobial susceptibility) and **137-150** (hemolysis) show the kinetic growth and hemolysis curves associated with each experimental endpoint depicted in **Figure 7**. Results of **Figure 7** are presented in standardized, quantified format in **Table S6**.

The FF-14 biphenyl motif contributes to increased outer and inner membrane permeabilization in gram-negative bacteria

To better characterize the mechanism underlying the contributions of the biphenyl motif to FF-14 antimicrobial activity, we carried out kinetic dual membrane permeabilization assays in *E. coli* and *P. aeruginosa* comparing the relative permeabilization of the outer (OM) and inner (IM) gram-negative membranes as measured by N-phenyl-naphthylamine (NPN) and propidium iodide (PI) staining over time in the presence of a range of concentrations of each of KR-12, FK-13, FF-14, and LL-37. This assay allows for the combination of both kinetics and raw levels of

permeabilization into a single composite metric of activity. As shown in **Figure 8A-B**, permeabilization was modest in the KR-12 derivative and increased sequentially through the addition of one (FK-13) and then two (FF-14) Phe residues to the N-terminus for both the OM and IM in both *E. coli* and *P. aeruginosa*, with FF-14 permeabilization activity approaching that of LL-37 itself. Thus, mimicry of the LL-37 N-terminus as in the placement of the biphenyl motif in FF-14 results in improved membrane permeabilization that more closely recapitulates that observed with LL-37.

While the single-point composite measure of peak permeabilization and kinetics used in **Figures 8A-B** gives a sense of the maximum permeabilization potential of each peptide, we were also interested in assessing permeabilization behavior at the functionally relevant limits of assay detection. Because the IM permeabilization of LL-37 consistently achieves at least 10% of its maximum value at concentrations at or below the corresponding MIC, we chose to define this 10% threshold as an internally calibrated minimum threshold of functionally relevant permeabilization.

On comparing the 10% threshold values for OM and IM permeabilization for each peptide with their corresponding MICs as in **Figure 8C**, we noted that, while all OM thresholds fall at or below the corresponding MIC, the ratio between the 10% threshold and the MIC is 4-8-fold greater for FF-14 than for LL-37. That is, while both display *E. coli* MICs in these studies of 3.1 μM, the FF-14 threshold value is 12.5 μM, while that for LL-37 is 1.6 μM. We have observed even larger gaps among LL-37 derivatives in *E. coli* in other studies[29]. Thus, despite the correlation between increased permeabilization in FF-14 and lower MICs, the antimicrobial activity of FF-14 and other cathelicidin derivatives may be more complex than membrane permeabilization alone. Kinetic curves associated with each condition are shown in **Figures S151-S154**.

Discussion

In this study, we build on our prior structure-activity work in full-length LL-37 to demonstrate that transposition of an N-terminal biphenyl motif onto the central LL-37 (18-29) activity region improves activity against gram-negative bacteria >16-fold. This is consistent with structural data from the same landmark study that first described LL-37 (18-29), also known as KR-12, which indicated that the four Phe residues of LL-37 are critical for interaction with model membranes[28]. The resultant short derivative, FF-14, better recapitulates the gram-negative and hemolytic activity of LL-37, which may make this a useful lead scaffold from which to build out peptidomimetic derivatives. Further work identifies stabilizing interventions such as the use of D-amino acids and C-amidation as well as selected N-lipidation moieties as potentially useful activity modulation strategies in the more active FF-14, as well as the portability of the biphenyl motif to longer cathelicidin scaffolds.

In addition to the importance of the LL-37 N-terminus for activity against gram-negative bacteria, our data suggest that primary sequence drives overall potency and toxicity in cathelicidin derivatives. Stabilizing modifications may prove necessary in downstream therapeutics, but neither these nor N-lipidation result in large changes in FF-14 activity. It is possible, however, that chemical modification may be more important for the modulation of primary sequences with lower intrinsic activity such as KR-12. Of note, while the studies here focus on the effects of N-terminal lipidation on the activity profiles of short cathelicidin derivatives, a separate question of interest is whether lipidation moieties placed at activity-neutral sites in these templates might yield favorable pharmacokinetic properties as in GLP-1 agonists. We have separately carried out a comprehensive mutagenesis to identify structure-promoting primary sequence modifications in FF-14, which may help to address this question[26].

Although the main focus of this study was on developing short derivatives like KR-12 with improved antimicrobial activity, a surprising finding shown here is that derivatives LL-25 and, to a lesser extent, GD-23 are both potent and substantially less hemolytic than LL-37. LL-

25 and GD-23 have both been described previously, but the separation between antimicrobial and hemolytic activity in these two peptides is, to our knowledge, a new finding[52]. Both LL-25 and GD-23 truncate prior to L28, which in our recent structure-activity studies in full-length LL-37 is one of the two critical residues required for oligomerization – the other being I24. Because I24 is retained in LL-25, GD-23, and FF-14[29], it may be possible to develop these derivatives as lead therapeutics through further detoxifying modifications around I24[26]. As demonstrated in **Figure 7**, the biphenyl pharmacophore is transferable to these longer cathelicidin scaffolds and substantially improves activity against *P. aeruginosa*.

The observation that primary sequence drives function in more active cathelicidin templates such as FF-14 raises the question of whether it might be possible to derive improved cathelicidin antimicrobials not only through rational design principles, but also through combinatorial chemistry. To this end, we have recently developed a methodology for the rapid synthesis and deconvolution of extremely large polyamide libraries on the order of up to 10^{18} members[9,56], which may allow for the directed evolution of synthetic cathelicidins as a complementary approach to the rational design approaches demonstrated here.

Cathelicidins are thought to act through membrane permeabilization, and our data in **Figure 8** demonstrate increased OM and IM permeabilization associated with the biphenyl pharmacophore. Although increased membrane permeabilization activity associated with the biphenyl motif is a likely driver of activity, we also noted that inner membrane permeabilization by FF-14 was detectable only to 12.5 μM in *E. coli* compared with an MIC of 3.1 μM (**Figure 8C**). By contrast, permeabilization by LL-37 is generally detectable at or below the equivalent MIC (*e.g.*, detectable inner membrane permeabilization to 1.6 μM for *E. coli* versus MIC of 3.1 μM). It is therefore possible that mechanisms underpinning the observed functional readouts may be more complex than membrane permeabilization alone, as we have expanded upon in related work[26,27,29].

Methods

Antimicrobial susceptibility testing –

Susceptibility testing was carried out based on previously described adaptations of CLSI methods modified for use with antimicrobial peptides. This includes the use of polypropylene plates as well as unadjusted Mueller Hinton Broth[57]. Methods were further miniaturized for use in 384-well plates at total volumes of either 35 or 50 µL. In brief, a 10x concentration of peptide was plated followed by the addition of a concentrated medium and cell mixture to yield a 1x mixture of peptide, medium, and cells. For example, if plating 50 µL, one would plate 5 µL of a 10x concentration of peptide followed by 45 µL of a 10/9 strength MHB and cell mixture. Plates were then monitored for absorbance at 600 nm for 18 hours at 37 °C at 30-minute intervals on a Tecan Spark plate reader, during which time they were housed in a large Tecan humidity cassette to minimize evaporation over the course of the experiment. Endpoint measures as depicted in main text figures are the final time point at 18 hours. Growth curves associated with these experiments can be found among the **Supplementary Figures**. Strains used throughout are antimicrobial susceptibility testing quality control strains, namely *E. coli* ATCC 25922 and *P. aeruginosa* ATCC 27853. Data within **Figures 1-2**, **4**, **6 / S87**, and **7** are from three independent experiments each.

Hemolysis assays –

Hemolysis assays were carried out by treating defibrinated sheep blood (Hardy Diagnostics) with each test peptide. In brief, peptides were prepared at a concentration of 500 µM in water and then diluted to 400 µM with 5x PBS. These were then serially diluted to the levels shown and plated at 25 µL per well in 384-well plates. To these peptides, we then added 25 µL of sheep blood washed to supernatant clearance for a final concentration of 0.5% v/v. Wells were then monitored at OD600 in a fashion similar to the methods used for antimicrobial susceptibility testing over 18 hours, which provides the kinetic curves shown in the

Supplementary Figures. At the end of 18 hours, 25 µL of PBS was added to each well followed by spinning of the 384-well plates for 10 minutes at 800 rcf. 25 µL of supernatant was then removed and added to a fresh 384-well plate for detection of free hemoglobin at 414 nm. Hemolysis controls throughout were thrice freeze-thawed blood from the same preparation used in plating, which were set to 100%. Data within **Figures 1-2**, **4**, **6 / S87**, and **7** are from three independent experiments each.

Dual membrane permeabilization assays –

Dual membrane permeabilization assays based on prior protocols (*e.g.* [58]) were carried out in M9+glucose with divalent cation concentrations adjusted to the levels present in the unadjusted MHB used for antimicrobial susceptibility testing in this study. In brief, cells were grown to OD600 of approximately 0.5 and then washed and resuspended in M9+glucose. To this cell suspension, we then added a final concentration of 10 µM N-phenyl-naphthylamine (NPN) and 5 µM propidium iodide (PI). We then added 50 µL of this mixture to 5 µL of 10x concentrated peptide over a range of concentrations in 384-well black, transparent bottom plates and monitored NPN (outer membrane permeabilization) at Ex 350 / Em 420 nm and PI (inner membrane permeabilization) at Ex 535 / Em 617 nm at 15-minute intervals over 4 hours at 37 °C in black. Quantification of fluorescence was scaled to that observed for LL-37. In brief, the average of cell background with no fluorophores added was subtracted from all wells. Fold-changes over no-peptide controls for each concentration of each peptide were then calculated. Finally, the highest fold-change within LL-37 was set to 100%, with remaining values scaled to this reference. These scaled values are shown in **Figures S151-154**. The single values shown in **Figure 8** represent a permeabilization index that is the product of the maximum permeabilization observed for each peptide and the proportion of the assay time required for that peptide to demonstrate at least 80% of its maximum level of permeabilization. Several of the high peptide wells in these experiments, particularly for FF-14, yielded signals over assay at

early timepoints. Where this occurs, the over assay timepoint was substituted with the next within-assay timepoint. The general effect of this is to underestimate the peaks of FF-14 permeabilization; no effect is expected on quantification of the lower limits of FF-14 permeabilization.

Peptide synthesis –

Peptides used in these studies were synthesized on automated flow synthesizers in a manner similar to those previously described[59–62]. Resin was 4-(4-hydroxymethyl-3-methoxyphenoxy)butyric acid (HMPB, ChemMatrix) except in the case of C-amidated peptides, where Rink Amide (ChemMatrix) was used. Cleavage was generally carried out by treating resin with Reagent K (82.5 % trifluoroacetic acid (TFA), 5% water, 5% phenol, 2.5% 1,2-ethanedithiol) for 2 hours at room temperature followed by precipitation with cold ether. Precipitated peptide was then resuspended in 50% water + 0.1% TFA / 50% acetonitrile + 0.1% TFA and lyophilized. Crude material was purified most commonly by reverse phase flash purification on a Biotage Selekt flash chromatography instrument with selected peptides purified by reverse phase high performance liquid chromatography. Analytical data associated with these syntheses are shown in **Figures S155-166** (associated with **Figure 1**), **167-176** (associated with **Figure 2**), **177-187** (associated with **Figure 4**), **188-193** (associated with **Figure 6**), **194-199** (associated with **Figure S87**), and **200-209** (associated with **Figure 7**). Peptides that are reused as controls across more than one experiment are grouped with the first figure in which they appear. Single-pass purifications were used throughout. Among the handful of instances in which this resulted in suboptimal purity – specifically among the **Figure S87** peptides – we did not note a biological signal to warrant any additional purification for further characterization.

Perfluoroaryl stapling –

Methods for stapling are based on those previously reported (*e.g.*, [19]). Intervals of *i,i+3* or *i,i+4* were stapled using hexafluorobenzene, while intervals of *i,i+7* were stapled with decafluorobiphenyl. In brief, peptide was dissolved to 1 mM in dimethylformamide (DMF) with the addition of stapling agent (2 mM final concentration for decafluorobiphenyl; 20 mM final concentration for hexafluorobenzene) and Tris to a final concentration of 30 mM. Reactions were then allowed to proceed for approximately 4-5 hours prior to dilution in water and purification by reverse phase flash chromatography.

Lipidation –

Lipidation was generally carried out via standard peptide bond formation procedures either in batch or by semi-automated flow synthesis[62] between the on-resin protected peptide and the carboxylic acid on each of the tails used in these studies (**Figure 5**). Cleavage then proceeded as per above for most moieties with selected exceptions for which alternatives such as Reagent B (88% TFA, 5% water, 5% phenol, 2% triisopropylsilane) were substituted.

Acknowledgements

This work has been funded by the National Institute of Allergy and Infectious Diseases (T32 AI007061 and K08 AI166345 to JSA; U19 AI142780 to BLP) and by the Cystic Fibrosis Foundation (ALBIN19F0, ALBIN21Q0, ALBIN22A0-KB to JSA).

Author Contributions

JSA designed and conducted experiments and wrote the paper. CJ and DAV conducted experiments. BLP guided experiments and wrote the paper.

Declaration of Interests

JSA declares no competing interests. BLP is a co-founder and/or member of the scientific advisory boards of several companies involved in peptide and protein therapeutics. Mass General Brigham Innovation has filed a provisional patent application associated with results described in this manuscript.

References

(1) Murray, C. J.; Ikuta, K. S.; Sharara, F.; Swetschinski, L.; Robles Aguilar, G.; Gray, A.; Han, C.; Bisignano, C.; Rao, P.; Wool, E.; Johnson, S. C.; Browne, A. J.; Chipeta, M. G.; Fell, F.; Hackett, S.; Haines-Woodhouse, G.; Kashef Hamadani, B. H.; Kumaran, E. A. P.; McManigal, B.; Agarwal, R.; Akech, S.; Albertson, S.; Amuasi, J.; Andrews, J.; Aravkin, A.; Ashley, E.; Bailey, F.; Baker, S.; Basnyat, B.; Bekker, A.; Bender, R.; Bethou, A.; Bielicki, J.; Boonkasidecha, S.; Bukosia, J.; Carvalheiro, C.; Castañeda-Orjuela, C.; Chansamouth, V.; Chaurasia, S.; Chiurchiù, S.; Chowdhury, F.; Cook, A. J.; Cooper, B.; Cressey, T. R.; Criollo-Mora, E.; Cunningham, M.; Darboe, S.; Day, N. P. J.; De Luca, M.; Dokova, K.; Dramowski, A.; Dunachie, S. J.; Eckmanns, T.; Eibach, D.; Emami, A.; Feasey, N.; Fisher-Pearson, N.; Forrest, K.; Garrett, D.; Gastmeier, P.; Giref, A. Z.; Greer, R. C.; Gupta, V.; Haller, S.; Haselbeck, A.; Hay, S. I.; Holm, M.; Hopkins, S.; Iregbu, K. C.; Jacobs, J.; Jarovsky, D.; Javanmardi, F.; Khorana, M.; Kissoon, N.; Kobeissi, E.; Kostyanev, T.; Krapp, F.; Krumkamp, R.; Kumar, A.; Kyu, H. H.; Lim, C.; Limmathurotsakul, D.; Loftus, M. J.; Lunn, M.; Ma, J.; Mturi, N.; Munera-Huertas, T.; Musicha, P.; Mussi-Pinhata, M. M.; Nakamura, T.; Nanavati, R.; Nangia, S.; Newton, P.; Ngoun, C.; Novotney, A.; Nwakanma, D.; Obiero, C. W.; Olivas-Martinez, A.; Olliaro, P.; Ooko, E.; Ortiz-Brizuela, E.; Peleg, A. Y.; Perrone, C.; Plakkal, N.; Ponce-de-Leon, A.; Raad, M.; Ramdin, T.; Riddell, A.; Roberts, T.; Robotham, J. V.; Roca, A.; Rudd, K. E.; Russell, N.; Schnall, J.; Scott, J. A. G.; Shivamallappa, M.; Sifuentes-Osornio, J.; Steenkeste, N.; Stewardson, A. J.; Stoeva, T.; Tasak, N.; Thaiprakong, A.; Thwaites, G.; Turner, C.; Turner, P.; van Doorn, H. R.; Velaphi, S.; Vongpradith, A.; Vu, H.; Walsh, T.; Waner, S.; Wangrangsimakul, T.; Wozniak, T.; Zheng, P.; Sartorius, B.; Lopez, A. D.; Stergachis, A.; Moore, C.; Dolecek, C.; Naghavi, M. Global Burden of Bacterial Antimicrobial Resistance in 2019: A Systematic Analysis. *The Lancet* **2022**, *399* (10325), 629–655. https://doi.org/10.1016/S0140-6736(21)02724-0/ATTACHMENT/B227DEB3-FF04-497F-82AC-637D8AB7F679/MMC1.PDF.

(2) Naghavi, M.; Vollset, S. E.; Ikuta, K. S.; Swetschinski, L. R.; Gray, A. P.; Wool, E. E.; Robles Aguilar, G.; Mestrovic, T.; Smith, G.; Han, C.; Hsu, R. L.; Chalek, J.; Araki, D. T.; Chung, E.; Raggi, C.; Gershberg Hayoon, A.; Davis Weaver, N.; Lindstedt, P. A.; Smith, A. E.; Altay, U.; Bhattacharjee, N. V; Giannakis, K.; Fell, F.; McManigal, B.; Ekapirat, N.; Mendes, J. A.; Runghien, T.; Srimokla, O.; Abdelkader, A.; Abd-Elsalam, S.; Aboagye, R. G.; Abolhassani, H.; Abualruz, H.; Abubakar, U.; Abukhadijah, H. J.; Aburuz, S.; Abu-Zaid, A.; Achalapong, S.; Addo, I. Y.; Adekanmbi, V.; Adeyeoluwa, T. E.; Adnani, Q. E. S.; Adzigbli, L. A.; Afzal, M. S.; Afzal, S.; Agodi, A.; Ahlstrom, A. J.; Ahmad, A.; Ahmad, S.; Ahmad, T.; Ahmadi, A.; Ahmed, A.; Ahmed, H.; Ahmed, I.; Ahmed, M.; Ahmed, S.; Ahmed, S. A.; Akkaif, M. A.; Al Awaidy, S.; Al Thaher, Y.; Alalalmeh, S. O.; AlBataineh, M. T.; Aldhaleei, W. A.; Al-Gheethi, A. A. S.; Alhaji, N. B.; Ali, A.; Ali, L.; Ali, S. S.; Ali, W.; Allel, K.; Al-Marwani, S.; Alrawashdeh, A.; Altaf, A.; Al-Tammemi, A. B.; Al-Tawfiq, J. A.; Alzoubi, K. H.; Al-Zyoud, W. A.; Amos, B.; Amuasi, J. H.; Ancuceanu, R.; Andrews, J. R.; Anil, A.; Anuoluwa, I. A.; Anvari, S.; Anyasodor, A. E.; Apostol, G. L. C.; Arabloo, J.; Arafat, M.; Aravkin, A. Y.; Areda, D.; Aremu, A.; Artamonov, A. A.; Ashley, E. A.; Asika, M. O.; Athari, S. S.; Atout, M. M. W.; Awoke, T.; Azadnajafabad, S.; Azam, J. M.; Aziz, S.; Azzam, A. Y.; Babaei, M.; Babin, F.-X.; Badar, M.; Baig, A. A.; Bajcetic, M.; Baker, S.; Bardhan, M.; Barqawi, H. J.; Basharat, Z.; Basiru, A.; Bastard, M.; Basu, S.; Bayleyegn, N. S.; Belete, M. A.; Bello, O. O.; Beloukas, A.; Berkley, J. A.; Bhagavathula, A. S.; Bhaskar, S.; Bhuyan, S. S.; Bielicki, J. A.; Briko, N. I.; Brown, C. S.; Browne, A. J.; Buonsenso, D.; Bustanji, Y.; Carvalheiro, C. G.; Castañeda-Orjuela, C. A.; Cenderadewi, M.; Chadwick, J.; Chakraborty, S.; Chandika, R. M.; Chandy, S.; Chansamouth, V.; Chattu, V. K.; Chaudhary, A. A.;

Ching, P. R.; Chopra, H.; Chowdhury, F. R.; Chu, D.-T.; Chutiyami, M.; Cruz-Martins, N.; da Silva, A. G.; Dadras, O.; Dai, X.; Darcho, S. D.; Das, S.; De la Hoz, F. P.; Dekker, D. M.; Dhama, K.; Diaz, D.; Dickson, B. F. R.; Djorie, S. G.; Dodangeh, M.; Dohare, S.; Dokova, K. G.; Doshi, O. P.; Dowou, R. K.; Dsouza, H. L.; Dunachie, S. J.; Dziedzic, A. M.; Eckmanns, T.; Ed-Dra, A.; Eftekharimehrabad, A.; Ekundayo, T. C.; El Sayed, I.; Elhadi, M.; El-Huneidi, W.; Elias, C.; Ellis, S. J.; Elsheikh, R.; Elsohaby, I.; Eltaha, C.; Eshrati, B.; Eslami, M.; Eyre, D. W.; Fadaka, A. O.; Fagbamigbe, A. F.; Fahim, A.; Fakhri-Demeshghieh, A.; Fasina, F. O.; Fasina, M. M.; Fatehizadeh, A.; Feasey, N. A.; Feizkhah, A.; Fekadu, G.; Fischer, F.; Fitriana, I.; Forrest, K. M.; Fortuna Rodrigues, C.; Fuller, J. E.; Gadanya, M. A.; Gajdács, M.; Gandhi, A. P.; Garcia-Gallo, E. E.; Garrett, D. O.; Gautam, R. K.; Gebregergis, M. W.; Gebrehiwot, M.; Gebremeskel, T. G.; Geffers, C.; Georgalis, L.; Ghazy, R. M.; Golechha, M.; Golinelli, D.; Gordon, M.; Gulati, S.; Gupta, R. Das; Gupta, S.; Gupta, V. K.; Habteyohannes, A. D.; Haller, S.; Harapan, H.; Harrison, M. L.; Hasaballah, A. I.; Hasan, I.; Hasan, R. S.; Hasani, H.; Haselbeck, A. H.; Hasnain, M. S.; Hassan, I. I.; Hassan, S.; Hassan Zadeh Tabatabaei, M. S.; Hayat, K.; He, J.; Hegazi, O. E.; Heidari, M.; Hezam, K.; Holla, R.; Holm, M.; Hopkins, H.; Hossain, M. M.; Hosseinzadeh, M.; Hostiuc, S.; Hussein, N. R.; Huy, L. D.; Ibáñez-Prada, E. D.; Ikiroma, A.; Ilic, I. M.; Islam, S. M. S.; Ismail, F.; Ismail, N. E.; Iwu, C. D.; Iwu-Jaja, C. J.; Jafarzadeh, A.; Jaiteh, F.; Jalilzadeh Yengejeh, R.; Jamora, R. D. G.; Javidnia, J.; Jawaid, T.; Jenney, A. W. J.; Jeon, H. J.; Jokar, M.; Jomehzadeh, N.; Joo, T.; Joseph, N.; Kamal, Z.; Kanmodi, K. K.; Kantar, R. S.; Kapisi, J. A.; Karaye, I. M.; Khader, Y. S.; Khajuria, H.; Khalid, N.; Khamesipour, F.; Khan, A.; Khan, M. J.; Khan, M. T.; Khanal, V.; Khidri, F. F.; Khubchandani, J.; Khusuwan, S.; Kim, M. S.; Kisa, A.; Korshunov, V. A.; Krapp, F.; Krumkamp, R.; Kuddus, M.; Kulimbet, M.; Kumar, D.; Kumaran, E. A. P.; Kuttikkattu, A.; Kyu, H. H.; Landires, I.; Lawal, B. K.; Le, T. T. T.; Lederer, I. M.; Lee, M.; Lee, S. W.; Lepape, A.; Lerango, T. L.; Ligade, V. S.; Lim, C.; Lim, S. S.; Limenh, L. W.; Liu, C.; Liu, X.; Liu, X.; Loftus, M. J.; M Amin, H. I.; Maass, K. L.; Maharaj, S. B.; Mahmoud, M. A.; Maikanti-Charalampous, P.; Makram, O. M.; Malhotra, K.; Malik, A. A.; Mandilara, G. D.; Marks, F.; Martinez-Guerra, B. A.; Martorell, M.; Masoumi-Asl, H.; Mathioudakis, A. G.; May, J.; McHugh, T. A.; Meiring, J.; Meles, H. N.; Melese, A.; Melese, E. B.; Minervini, G.; Mohamed, N. S.; Mohammed, S.; Mohan, S.; Mokdad, A. H.; Monasta, L.; Moodi Ghalibaf, A.; Moore, C. E.; Moradi, Y.; Mossialos, E.; Mougin, V.; Mukoro, G. D.; Mulita, F.; Muller-Pebody, B.; Murillo-Zamora, E.; Musa, S.; Musicha, P.; Musila, L. A.; Muthupandian, S.; Nagarajan, A. J.; Naghavi, P.; Nainu, F.; Nair, T. S.; Najmuldeen, H. H. R.; Natto, Z. S.; Nauman, J.; Nayak, B. P.; Nchanji, G. T.; Ndishimye, P.; Negoi, I.; Negoi, R. I.; Nejadghaderi, S. A.; Nguyen, Q. P.; Noman, E. A.; Nwakanma, D. C.; O'Brien, S.; Ochoa, T. J.; Odetokun, I. A.; Ogundijo, O. A.; Ojo-Akosile, T. R.; Okeke, S. R.; Okonji, O. C.; Olagunju, A. T.; Olivas-Martinez, A.; Olorukooba, A. A.; Olwoch, P.; Onyedibe, K. I.; Ortiz-Brizuela, E.; Osuolale, O.; Ounchanum, P.; Oyeyemi, O. T.; P A, M. P.; Paredes, J. L.; Parikh, R. R.; Patel, J.; Patil, S.; Pawar, S.; Peleg, A. Y.; Peprah, P.; Perdigão, J.; Perrone, C.; Petcu, I.-R.; Phommasone, K.; Piracha, Z. Z.; Poddighe, D.; Pollard, A. J.; Poluru, R.; Ponce-De-Leon, A.; Puvvula, J.; Qamar, F. N.; Qasim, N. H.; Rafai, C. D.; Raghav, P.; Rahbarnia, L.; Rahim, F.; Rahimi-Movaghar, V.; Rahman, M.; Rahman, M. A.; Ramadan, H.; Ramasamy, S. K.; Ramesh, P. S.; Ramteke, P. W.; Rana, R. K.; Rani, U.; Rashidi, M.-M.; Rathish, D.; Rattanavong, S.; Rawaf, S.; Redwan, E. M. M.; Reyes, L. F.; Roberts, T.; Robotham, J. V; Rosenthal, V. D.; Ross, A. G.; Roy, N.; Rudd, K. E.; Sabet, C. J.; Saddik, B. A.; Saeb, M. R.; Saeed, U.; Saeedi Moghaddam, S.; Saengchan, W.; Safaei, M.; Saghazadeh, A.; Saheb Sharif-Askari, N.; Sahebkar, A.; Sahoo, S. S.; Sahu, M.; Saki, M.; Salam, N.; Saleem, Z.; Saleh, M. A.; Samodra, Y. L.; Samy, A. M.; Saravanan, A.; Satpathy, M.; Schumacher, A. E.; Sedighi, M.;

Seekaew, S.; Shafie, M.; Shah, P. A.; Shahid, S.; Shahwan, M. J.; Shakoor, S.; Shalev, N.; Shamim, M. A.; Shamshirgaran, M. A.; Shamsi, A.; Sharifan, A.; Shastry, R. P.; Shetty, M.; Shittu, A.; Shrestha, S.; Siddig, E. E.; Sideroglou, T.; Sifuentes-Osornio, J.; Silva, L. M. L. R.; Simões, E. A. F.; Simpson, A. J. H.; Singh, A.; Singh, S.; Sinto, R.; Soliman, S. S. M.; Soraneh, S.; Stoesser, N.; Stoeva, T. Z.; Swain, C. K.; Szarpak, L.; T Y, S. S.; Tabatabai, S.; Tabche, C.; Taha, Z. M.-A.; Tan, K.-K.; Tasak, N.; Tat, N. Y.; Thaiprakong, A.; Thangaraju, P.; Tigoi, C. C.; Tiwari, K.; Tovani-Palone, M. R.; Tran, T. H.; Tumurkhuu, M.; Turner, P.; Udoakang, A. J.; Udoh, A.; Ullah, N.; Ullah, S.; Vaithinathan, A. G.; Valenti, M.; Vos, T.; Vu, H. T. L.; Waheed, Y.; Walker, A. S.; Walson, J. L.; Wangrangsimakul, T.; Weerakoon, K. G.; Wertheim, H. F. L.; Williams, P. C. M.; Wolde, A. A.; Wozniak, T. M.; Wu, F.; Wu, Z.; Yadav, M. K. K.; Yaghoubi, S.; Yahaya, Z. S.; Yarahmadi, A.; Yezli, S.; Yismaw, Y. E.; Yon, D. K.; Yuan, C.-W.; Yusuf, H.; Zakham, F.; Zamagni, G.; Zhang, H.; Zhang, Z.-J.; Zielińska, M.; Zumla, A.; Zyoud, S. H. H.; Zyoud, S. H.; Hay, S. I.; Stergachis, A.; Sartorius, B.; Cooper, B. S.; Dolecek, C.; Murray, C. J. L. Global Burden of Bacterial Antimicrobial Resistance 1990-2021: A Systematic Analysis with Forecasts to 2050. *Lancet* **2024**, *404* (10459), 1199–1226. https://doi.org/10.1016/S0140-6736(24)01867-1.

(3) Wang, G.; Li, X.; Wang, Z. APD3: The Antimicrobial Peptide Database as a Tool for Research and Education. *Nucleic Acids Res.* **2016**, *44* (D1), D1087–D1093. https://doi.org/10.1093/nar/gkv1278.

(4) Magana, M.; Pushpanathan, M.; Santos, A. L.; Leanse, L.; Fernandez, M.; Ioannidis, A.; Giulianotti, M. A.; Apidianakis, Y.; Bradfute, S.; Ferguson, A. L.; Cherkasov, A.; Seleem, M. N.; Pinilla, C.; de la Fuente-Nunez, C.; Lazaridis, T.; Dai, T.; Houghten, R. A.; Hancock, R. E. W.; Tegos, G. P. The Value of Antimicrobial Peptides in the Age of Resistance. *Lancet Infect. Dis.* **2020**, *20* (9), e216–e230. https://doi.org/10.1016/S1473-3099(20)30327-3.

(5) Hancock, R. E. W.; Haney, E. F.; Gill, E. E. The Immunology of Host Defence Peptides: Beyond Antimicrobial Activity. *Nat. Rev. Immunol.* **2016**, *16* (5), 321–334. https://doi.org/10.1038/nri.2016.29.

(6) Haney, E. F.; Straus, S. K.; Hancock, R. E. W. Reassessing the Host Defense Peptide Landscape. *Front. Chem.* **2019**, *7*, 43. https://doi.org/10.3389/fchem.2019.00043.

(7) Nan, Y. H.; Bang, J. K.; Jacob, B.; Park, I. S.; Shin, S. Y. Prokaryotic Selectivity and LPS-Neutralizing Activity of Short Antimicrobial Peptides Designed from the Human Antimicrobial Peptide LL-37. *Peptides (N.Y.).* **2012**, *35* (2), 239–247. https://doi.org/10.1016/J.PEPTIDES.2012.04.004.

(8) Nell, M. J.; Tjabringa, G. S.; Wafelman, A. R.; Verrijk, R.; Hiemstra, P. S.; Drijfhout, J. W.; Grote, J. J. Development of Novel LL-37 Derived Antimicrobial Peptides with LPS and LTA Neutralizing and Antimicrobial Activities for Therapeutic Application. *Peptides (N.Y.).* **2006**, *27* (4), 649–660. https://doi.org/10.1016/J.PEPTIDES.2005.09.016.

(9) Albin, J. S.; Lee, G. Y.; Johnson, C.; Vithanage, D. A.; Vuong, W.; Pentelute, B. L. Rapid Generation of Hypervariable Chemical Libraries. *Chem* **2025**, *0* (0), 102501. https://doi.org/10.1016/J.CHEMPR.2025.102501.

(10) Ma, X.; Aminov, R.; Franco, O. L.; de la Fuente-Nunez, C.; Wang, G.; Wang, J. Editorial: Antimicrobial Peptides and Their Druggability, Bio-Safety, Stability, and Resistance. *Front. Microbiol.* **2024**, *15*. https://doi.org/10.3389/FMICB.2024.1425952.

(11) Friedman, J. M. The Discovery and Development of GLP-1 Based Drugs That Have Revolutionized the Treatment of Obesity. *Proc. Natl. Acad. Sci. U. S. A.* **2024**, *121* (39), e2415550121. https://doi.org/10.1073/PNAS.2415550121.

(12) Dürr, U. H. N.; Sudheendra, U. S.; Ramamoorthy, A. LL-37, the Only Human Member of the Cathelicidin Family of Antimicrobial Peptides. *Biochimica et Biophysica Acta (BBA) - Biomembranes* **2006**, *1758* (9), 1408–1425. https://doi.org/10.1016/J.BBAMEM.2006.03.030.

(13) Turner, J.; Cho, Y.; Dinh, N. N.; Waring, A. J.; Lehrer, R. I. Activities of LL-37, a Cathelin-Associated Antimicrobial Peptide of Human Neutrophils. *Antimicrob. Agents Chemother.* **1998**, *42* (9), 2206–2214.

(14) De Yang; Chen, Q.; Schmidt, A. P.; Anderson, G. M.; Wang, J. M.; Wooters, J.; Oppenheim, J. J.; Chertov, O. Ll-37, the Neutrophil Granule–And Epithelial Cell–Derived Cathelicidin, Utilizes Formyl Peptide Receptor–Like 1 (Fprl1) as a Receptor to Chemoattract Human Peripheral Blood Neutrophils, Monocytes, and T Cells. *J. Exp. Med.* **2000**, *192* (7), 1069–1074. https://doi.org/10.1084/jem.192.7.1069.

(15) Wan, M.; van der Does, A. M.; Tang, X.; Lindbom, L.; Agerberth, B.; Haeggström, J. Z. Antimicrobial Peptide LL-37 Promotes Bacterial Phagocytosis by Human Macrophages. *J. Leukoc. Biol.* **2014**, *95* (6), 971–981. https://doi.org/10.1189/jlb.0513304.

(16) Mookherjee, N.; Lippert, D. N. D.; Hamill, P.; Falsafi, R.; Nijnik, A.; Kindrachuk, J.; Pistolic, J.; Gardy, J.; Miri, P.; Naseer, M.; Foster, L. J.; Hancock, R. E. W. Intracellular Receptor for Human Host Defense Peptide LL-37 in Monocytes. *The Journal of Immunology* **2009**, *183* (4), 2688–2696. https://doi.org/10.4049/jimmunol.0802586.

(17) De Yang, B.; Chen, Q.; Schmidt, A. P.; Anderson, G. M.; Wang, J. M.; Wooters, J.; Oppenheim, J. J.; Chertov, O. LL-37, the Neutrophil Granule- and Epithelial Cell-Derived Cathelicidin, Utilizes Formyl Peptide Receptor-like 1 (FPRL1) as a Receptor to Chemoattract Human Peripheral Blood Neutrophils, Monocytes, and T Cells. *Journal of Experimental Medicine* **2000**, *192* (7), 1069–1074. https://doi.org/10.1084/jem.192.7.1069.

(18) Cirioni, O.; Giacometti, A.; Ghiselli, R.; Bergnach, C.; Orlando, F.; Silvestri, C.; Mocchegiani, F.; Licci, A.; Skerlavaj, B.; Rocchi, M.; Saba, V.; Zanetti, M.; Scalise, G. LL-37 Protects Rats against Lethal Sepsis Caused by Gram-Negative Bacteria. *Antimicrob. Agents Chemother.* **2006**, *50* (5), 1672–1679. https://doi.org/10.1128/AAC.50.5.1672-1679.2006.

(19) Spokoyny, A. M.; Zou, Y.; Ling, J. J.; Yu, H.; Lin, Y.-S.; Pentelute, B. L. A Perfluoroaryl-Cysteine S N Ar Chemistry Approach to Unprotected Peptide Stapling. **2013**. https://doi.org/10.1021/ja400119t.

(20) Mourtada, R.; Herce, H. D.; Yin, D. J.; Moroco, J. A.; Wales, T. E.; Engen, J. R.; Walensky, L. D. Design of Stapled Antimicrobial Peptides That Are Stable, Nontoxic and Kill Antibiotic-Resistant Bacteria in Mice. *Nat. Biotechnol.* **2019**, *37* (10), 1186–1197. https://doi.org/10.1038/s41587-019-0222-z.

(21) Schissel, C. K.; Farquhar, C. E.; Malmberg, A. B.; Loas, A.; Pentelute, B. L. Cell-Penetrating d -Peptides Retain Antisense Morpholino Oligomer Delivery Activity. *ACS Bio and Med Chem Au*

2022, *2* (2), 150–160. https://doi.org/10.1021/ACSBIOMEDCHEMAU.1C00053/ASSET/IMAGES/MEDIUM/BG1C00053_M001.GIF.

(22) Kurtzhals, P.; Østergaard, S.; Nishimura, E.; Kjeldsen, T. Derivatization with Fatty Acids in Peptide and Protein Drug Discovery. *Nature Reviews Drug Discovery 2022 22:1* **2022**, *22* (1), 59–80. https://doi.org/10.1038/s41573-022-00529-w.

(23) Burton, M. F.; Steel, P. G. The Chemistry and Biology of LL-37. *Nat. Prod. Rep.* **2009**, *26* (12), 1572–1584. https://doi.org/10.1039/B912533G.

(24) Srinivas, N.; Jetter, P.; Ueberbacher, B. J.; Werneburg, M.; Zerbe, K.; Steinmann, J.; Van der Meijden, B.; Bernardini, F.; Lederer, A.; Dias, R. L. A.; Misson, P. E.; Henze, H.; Zumbrunn, J.; Gombert, F. O.; Obrecht, D.; Hunziker, P.; Schauer, S.; Ziegler, U.; Käch, A.; Eberl, L.; Riedel, K.; DeMarco, S. J.; Robinson, J. A. Peptidomimetic Antibiotics Target Outer-Membrane Biogenesis in Pseudomonas Aeruginosa. *Science* **2010**, *327* (5968), 1010–1013. https://doi.org/10.1126/science.1182749.

(25) Martin-Loeches, I.; Dale, G. E.; Torres, A. Murepavadin: A New Antibiotic Class in the Pipeline. *Expert Rev. Anti. Infect. Ther.* **2018**, *16* (4), 259–268. https://doi.org/10.1080/14787210.2018.1441024.

(26) Albin, J. S.; Pentelute, B. L. Paired Helix Scanning Distinguishes Structural Requirements for Amphipathic Peptide Scaffold Functions. *bioRxiv* **2026**, 2025.05.22.655621. https://doi.org/10.1101/2025.05.22.655621.

(27) Albin, J. S.; Vithanage, D. A.; Vuong, W.; Johnson, C.; Pentelute, B. L. Modulation of the Human Cathelicidin Dimerization Interface Separates Antimicrobial Activity from Mammalian Membrane Disruption. *bioRxiv* **2026**, 2026.02.13.705689. https://doi.org/10.64898/2026.02.13.705689.

(28) Wang, G. Structures of Human Host Defense Cathelicidin LL-37 and Its Smallest Antimicrobial Peptide KR-12 in Lipid Micelles. *Journal of Biological Chemistry* **2008**, *283* (47), 32637–32643. https://doi.org/10.1074/JBC.M805533200.

(29) Albin, J. S.; Vithanage, D. A.; Vuong, W.; Johnson, C.; Yonker, L. M.; Pentelute, B. L. Separability of Antibacterial and Membranolytic Activity in the Human Host Defense Peptide LL-37. *bioRxiv* **2025**, 2025.05.22.655608. https://doi.org/10.1101/2025.05.22.655608.

(30) Agerberth, B.; Gunne, H.; Odeberg, J.; Kogner, P.; Boman, H. G.; Gudmundsson, G. H. PR-39, a Proline-Rich Peptide Antibiotic from Pig, and FALL-39, a Tentative Human Counterpart. *Vet. Immunol. Immunopathol.* **1996**, *54* (1–4), 127–131. https://doi.org/10.1016/S0165-2427(96)05676-0.

(31) Agerberth, B.; Gunne, H.; Odeberg, J.; Kogner, P.; Boman, H. G.; Gudmundsson, G. H. FALL-39, a Putative Human Peptide Antibiotic, Is Cysteine-Free and Expressed in Bone Marrow and Testis. *Proc. Natl. Acad. Sci. U. S. A.* **1995**, *92* (1), 195–199. https://doi.org/10.1073/PNAS.92.1.195.

(32) Gudmundsson, G. H.; Magnusson, K. P.; Chowdhary, B. P.; Johansson, M.; Andersson, L.; Boman, H. G. Structure of the Gene for Porcine Peptide Antibiotic PR-39, a Cathelin Gene Family

Member: Comparative Mapping of the Locus for the Human Peptide Antibiotic FALL-39. *Proceedings of the National Academy of Sciences* **1995**, *92* (15), 7085–7089. https://doi.org/10.1073/PNAS.92.15.7085.

(33) Gudmundsson, G. H.; Agerberth, B.; Odeberg, J.; Bergman, T.; Olsson, B.; Salcedo, R. The Human Gene FALL39 and Processing of the Cathelin Precursor to the Antibacterial Peptide LL-37 in Granulocytes. *Eur. J. Biochem.* **1996**, *238* (2), 325–332. https://doi.org/10.1111/J.1432-1033.1996.0325Z.X.

(34) Jacob, B.; Park, I. S.; Bang, J. K.; Shin, S. Y. Short KR-12 Analogs Designed from Human Cathelicidin LL-37 Possessing Both Antimicrobial and Antiendotoxic Activities without Mammalian Cell Toxicity. *J. Pept. Sci.* **2013**, *19* (11), 700–707. https://doi.org/10.1002/PSC.2552.

(35) Kim, E. Y.; Rajasekaran, G.; Shin, S. Y. LL-37-Derived Short Antimicrobial Peptide KR-12-A5 and Its D-Amino Acid Substituted Analogs with Cell Selectivity, Anti-Biofilm Activity, Synergistic Effect with Conventional Antibiotics, and Anti-Inflammatory Activity. *Eur. J. Med. Chem.* **2017**, *136*, 428–441. https://doi.org/10.1016/j.ejmech.2017.05.028.

(36) Muhammad, T.; Strömstedt, A. A.; Gunasekera, S.; Göransson, U. Transforming Cross-Linked Cyclic Dimers of KR-12 into Stable and Potent Antimicrobial Drug Leads. *Biomedicines* **2023**, *11* (2). https://doi.org/10.3390/BIOMEDICINES11020504.

(37) Blasi-Romero, A.; Ångström, M.; Franconetti, A.; Muhammad, T.; Jiménez-Barbero, J.; Göransson, U.; Palo-Nieto, C.; Ferraz, N. KR-12 Derivatives Endow Nanocellulose with Antibacterial and Anti-Inflammatory Properties: Role of Conjugation Chemistry. *ACS Appl. Mater. Interfaces* **2023**, *15* (20), 24186–24196. https://doi.org/10.1021/ACSAMI.3C04237/ASSET/IMAGES/LARGE/AM3C04237_0006.JPEG.

(38) Ajish, C.; Yang, S.; Kumar, S. D.; Kim, E. Y.; Min, H. J.; Lee, C. W.; Shin, S. H.; Shin, S. Y. A Novel Hybrid Peptide Composed of LfcinB6 and KR-12-A4 with Enhanced Antimicrobial, Anti-Inflammatory and Anti-Biofilm Activities. *Scientific Reports 2022 12:1* **2022**, *12* (1), 4365-. https://doi.org/10.1038/s41598-022-08247-4.

(39) Zhang, Y.; Zheng, M.; Wang, Z.; Liu, Z.; Chen, S.; Li, X.; Shi, Y.; Hu, H. Discovery of Novel Antibacterial Agent for the Infected Wound Treatment: All-Hydrocarbon Stapling Optimization of LL-37. *Theranostics* **2024**, *14* (3), 1181. https://doi.org/10.7150/THNO.87916.

(40) Mishra, B.; Epand, R. F.; Epand, R. M.; Wang, G. Structural Location Determines Functional Roles of the Basic Amino Acids of KR-12, the Smallest Antimicrobial Peptide from Human Cathelicidin LL-37. *RSC Adv.* **2013**, *3* (42), 19560–19571. https://doi.org/10.1039/C3RA42599A.

(41) Gunasekera, S.; Muhammad, T.; Strömstedt, A. A.; Rosengren, K. J.; Göransson, U. Alanine and Lysine Scans of the LL-37-Derived Peptide Fragment KR-12 Reveal Key Residues for Antimicrobial Activity. *Chembiochem* **2018**, *19* (9), 931–939. https://doi.org/10.1002/CBIC.201700599.

(42) Lakshmaiah Narayana, J.; Mechesso, A. F.; Rather, I. I. G.; Zarena, D.; Luo, J.; Xie, J.; Wang, G. Origami of KR-12 Designed Antimicrobial Peptides and Their Potential Applications. *Antibiotics* **2024**, *13* (9), 816. https://doi.org/10.3390/ANTIBIOTICS13090816/S1.

(43) Kamysz, E.; Sikorska, E.; Bauer, M.; Sikora, K.; Neubauer, D. Influence of Lipidation Pattern of the KR12 Fragment of Peptide LL-37 on Its Antibacterial and Hemolytic Activities. *Int. J. Mol. Sci.* **2023**, *24* (6), 5505. https://doi.org/10.3390/IJMS24065505/S1.

(44) Kamysz, E.; Sikorska, E.; Jaśkiewicz, M.; Bauer, M.; Neubauer, D.; Bartoszewska, S.; Barańska-Rybak, W.; Kamysz, W. Lipidated Analogs of the LL-37-Derived Peptide Fragment KR12—Structural Analysis, Surface-Active Properties and Antimicrobial Activity. *International Journal of Molecular Sciences 2020, Vol. 21, Page 887* **2020**, *21* (3), 887. https://doi.org/10.3390/IJMS21030887.

(45) Lakshmaiah Narayana, J.; Golla, R.; Mishra, B.; Wang, X.; Lushnikova, T.; Zhang, Y.; Verma, A.; Kumar, V.; Xie, J.; Wang, G. Short and Robust Anti-Infective Lipopeptides Engineered Based on the Minimal Antimicrobial Peptide KR12 of Human LL-37. *ACS Infect. Dis.* **2021**, *7* (6), 1795–1808. https://doi.org/10.1021/ACSINFECDIS.1C00101/SUPPL_FILE/ID1C00101_SI_001.PDF.

(46) Wang, G.; Hanke, M. L.; Mishra, B.; Lushnikova, T.; Heim, C. E.; Thomas, V. C.; Bayles, K. W.; Kielian, T. Transformation of Human Cathelicidin LL-37 into Selective, Stable, and Potent Antimicrobial Compounds. *ACS Chem. Biol.* **2014**, *9* (9), 1997–2002. https://doi.org/10.1021/CB500475Y/SUPPL_FILE/CB500475Y_SI_001.PDF.

(47) Li, X.; Li, Y.; Han, H.; Miller, D. W.; Wang, G. Solution Structures of Human Ll-37 Fragments and NMR-Based Identification of a Minimal Membrane-Targeting Antimicrobial and Anticancer Region. *J. Am. Chem. Soc.* **2006**, *128* (17), 5776–5785. https://doi.org/10.1021/JA0584875/SUPPL_FILE/JA0584875SI20051222_013003.PDF.

(48) *CLSI eClipse Ultimate Access - Powered by Edaptive Technologies*. https://em100.edaptivedocs.net/Login.aspx?ru=1&emsg=275 (accessed 2025-05-07).

(49) Li, X.; Li, Y.; Han, H.; Miller, D. W.; Wang, G. Solution Structures of Human Ll-37 Fragments and NMR-Based Identification of a Minimal Membrane-Targeting Antimicrobial and Anticancer Region. *J. Am. Chem. Soc.* **2006**, *128* (17), 5776–5785. https://doi.org/10.1021/JA0584875/SUPPL_FILE/JA0584875SI20051222_013003.PDF.

(50) Tai, K. P.; Le, V. V.; Selsted, M. E.; Ouellette, A. J. Hydrophobic Determinants of α-Defensin Bactericidal Activity. *Infect. Immun.* **2014**, *82* (6), 2195–2202. https://doi.org/10.1128/IAI.01414-13.

(51) Dean, S. N.; Bishop, B. M.; Van Hoek, M. L. Susceptibility of Pseudomonas Aeruginosa Biofilm to Alpha-Helical Peptides: D-Enantiomer of LL-37. *Front. Microbiol.* **2011**, *2* (JULY), 10301. https://doi.org/10.3389/FMICB.2011.00128/BIBTEX.

(52) Braff, M. H.; Hawkins, M. A.; Nardo, A. Di; Lopez-Garcia, B.; Howell, M. D.; Wong, C.; Lin, K.; Streib, J. E.; Dorschner, R.; Leung, D. Y. M.; Gallo, R. L. Structure-Function Relationships among Human Cathelicidin Peptides: Dissociation of Antimicrobial Properties from Host Immunostimulatory Activities. *J. Immunol.* **2005**, *174* (7), 4271–4278. https://doi.org/10.4049/JIMMUNOL.174.7.4271.

(53) Kamysz, E.; Sikorska, E.; Jaśkiewicz, M.; Bauer, M.; Neubauer, D.; Bartoszewska, S.; Barańska-Rybak, W.; Kamysz, W. Lipidated Analogs of the Ll-37-Derived Peptide Fragment KR12—

Structural Analysis, Surface-Active Properties and Antimicrobial Activity. *Int. J. Mol. Sci.* **2020**, *21* (3). https://doi.org/10.3390/ijms21030887.

(54) Kamysz, E.; Sikorska, E.; Bauer, M.; Sikora, K.; Neubauer, D. Influence of Lipidation Pattern of the KR12 Fragment of Peptide LL-37 on Its Antibacterial and Hemolytic Activities. *Int. J. Mol. Sci.* **2023**, *24* (6), 5505. https://doi.org/10.3390/IJMS24065505/S1.

(55) Wang, Z.; Koirala, B.; Hernandez, Y.; Zimmerman, M.; Park, S.; Perlin, D. S.; Brady, S. F. A Naturally Inspired Antibiotic to Target Multidrug-Resistant Pathogens. *Nature 2022 601:7894* **2022**, *601* (7894), 606–611. https://doi.org/10.1038/s41586-021-04264-x.

(56) Johnson, C.; Vithanage, D. A.; Lee, G. Y.; Pentelute, B. L.; Albin, J. S. Automated Flow Synthesis of Combinatorial Protein Libraries. **2025**. https://doi.org/10.26434/CHEMRXIV-2025-MN6CT.

(57) Wiegand, I.; Hilpert, K.; Hancock, R. E. W. Agar and Broth Dilution Methods to Determine the Minimal Inhibitory Concentration (MIC) of Antimicrobial Substances. *Nat. Protoc.* **2008**, *3* (2), 163–175. https://doi.org/10.1038/nprot.2007.521.

(58) Ma, B.; Fang, C.; Zhang, J.; Wang, M.; Luo, X.; Hou, Z. Contemporaneous Measurement of Outer and Inner Membrane Permeability in Gram-Negative Bacteria. *Bio. Protoc.* **2020**, *10* (5). https://doi.org/10.21769/bioprotoc.3548.

(59) Albin, J. S.; Pentelute, B. L. Efficient Flow Synthesis of Human Antimicrobial Peptides. *Aust. J. Chem.* **2020**, *73* (4), 380–388. https://doi.org/10.1071/CH20043.

(60) Hartrampf, N.; Saebi, A.; Poskus, M.; Gates, Z. P.; Callahan, A. J.; Cowfer, A. E.; Hanna, S.; Antilla, S.; Schissel, C. K.; Quartararo, A. J.; Ye, X.; Mijalis, A. J.; Simon, M. D.; Loas, A.; Liu, S.; Jessen, C.; Nielsen, T. E.; Pentelute, B. L. Synthesis of Proteins by Automated Flow Chemistry. *Science (1979).* **2020**, *368* (6494), 980–987. https://doi.org/10.1126/science.abb2491.

(61) Mijalis, A. J.; Thomas, D. A.; Simon, M. D.; Adamo, A.; Beaumont, R.; Jensen, K. F.; Pentelute, B. L. A Fully Automated Flow-Based Approach for Accelerated Peptide Synthesis. *Nat. Chem. Biol.* **2017**, *13* (5), 464–466. https://doi.org/10.1038/nchembio.2318.

(62) Simon, M. D.; Heider, P. L.; Adamo, A.; Vinogradov, A. A.; Mong, S. K.; Li, X.; Berger, T.; Policarpo, R. L.; Zhang, C.; Zou, Y.; Liao, X.; Spokoyny, A. M.; Jensen, K. F.; Pentelute, B. L. Rapid Flow-Based Peptide Synthesis. *ChemBioChem* **2014**, *15* (5), 713–720. https://doi.org/10.1002/cbic.201300796.

A.

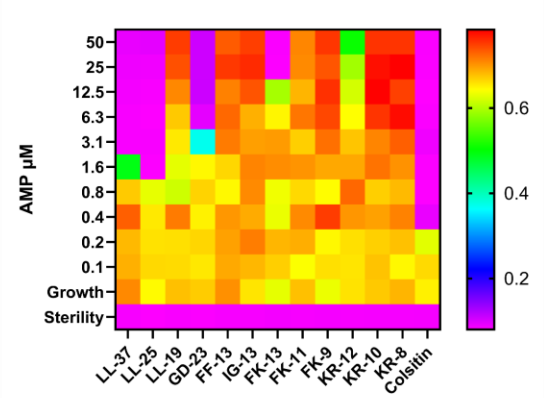

B.

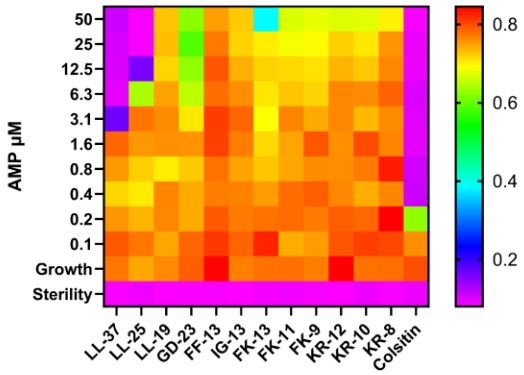

C.

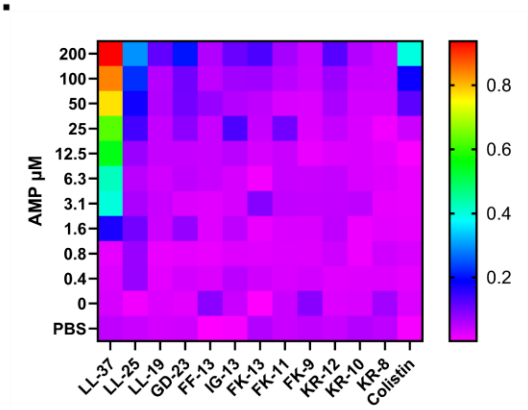

D.

```
LL-37     LLGDFFRKSKEKIGKEFKRIVQRIKDFLRNLVPRTES   37
LL-25     LLGDFFRKSKEKIGKEFKRIVQRIK------------   25
LL-19     LLGDFFRKSKEKIGKEFKR------------------   19
GD-23     --GDFFRKSKEKIGKEFKRIVQRIK------------   23
FF-13     ----FFRKSKEKIGKEF--------------------   13
IG-13     ------------IGKEFKRIVQRIK------------   13
FK-13     ----------------FKRIVQRIKDFLR--------   13
FK-11     ----------------FKRIVQRIKDF----------   11
FK-9      ----------------FKRIVQRIK------------   9
KR-12     -----------------KRIVQRIKDFLR--------   12
KR-10     -----------------KRIVQRIKDF----------   10
KR-8      -----------------KRIVQRIK------------   8
```

Figure 1 – Limited activity of shorter derivatives of LL-37. A. Antimicrobial susceptibility testing showing the activity of each derivative as well as a colistin control for reference against *E. coli* (ATCC 25922). In the heatmap plate depiction, cooler colors indicate low or absent bacterial growth as detected by the OD600 measured at 18 hours of incubation at 37 °C. **B.** As in **A.**, but with *P. aeruginosa* (ATCC 27853). **C.** Hemolysis assays in which defibrinated sheep blood in PBS was incubated with the indicated peptide for 18 hours at 37 °C with subsequent quantification of hemoglobin released into the supernatant at 414 nm. Cool colors indicate little or no release of hemoglobin, where all levels are scaled to 100% hemolysis freeze-thaw controls. Levels throughout are the mean of three independent experiments. **D.** Alignment showing the sequence of LL-37 in comparison with shorter derivatives tested in initial studies, which have been described previously.

A.

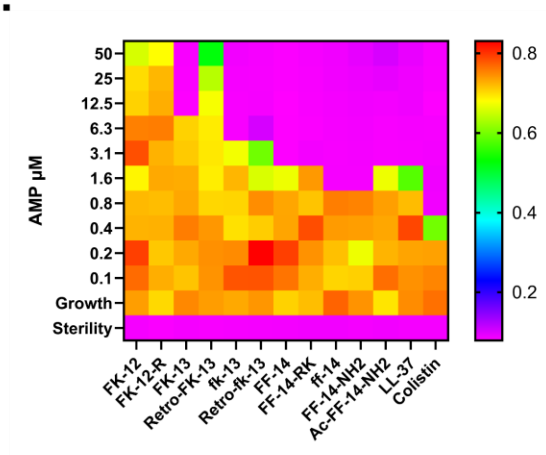

B.

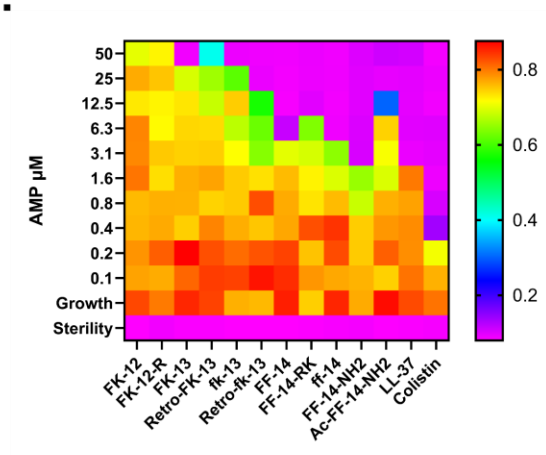

C.

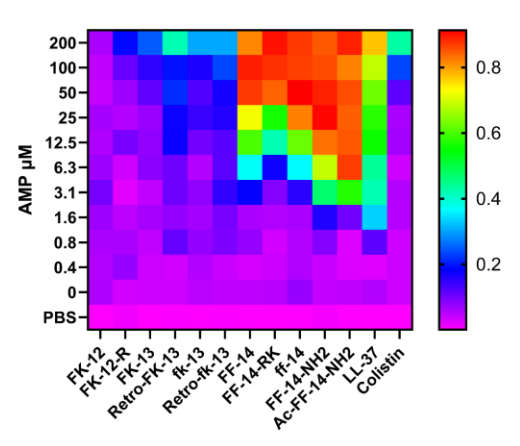

D.

FK-12	-FKRIVQRIKDFL
FK-12-R	-FKRIVQRIKDF-R
FK-13	-FKRIVQRIKDFLR
Retro-FK-13	-RLFDKIRQVIRKF
fk-13	-fkrivqrikdflr
Retro fk-13	-rlfdkirqvirkf
FF-14	FFKRIVQRIKDFLR
FF-14-RK	FFRKIVQRIKDFLR
ff-14	ffkrivqrikdflr
FF-14-NH_2	FFKRIVQRIKDFLR-NH_2
Ac-FF-14-NH_2	Ac-FFKRIVQRIKDFLR-NH_2
LL-37	LLGD**FFRK**SKEKIGK**EFKR**IVQRIKDFLRNLVPRTES

E.

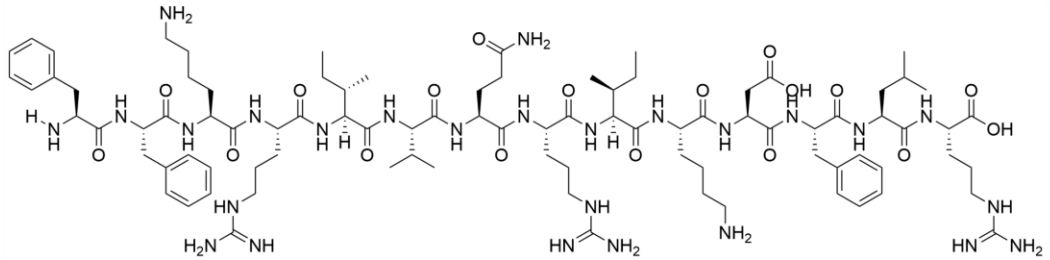

Figure 2 – Mimicry of the LL-37 N-terminus yields a 14-mer with activity comparable to full-length LL-37. A. Antimicrobial susceptibility testing showing the activity of each derivative as well as a colistin control against *E. coli* (ATCC 25922). In the heatmap plate depiction, cooler colors indicate low or absent bacterial growth as detected by the OD600 measure at 18 hours of incubation at 37 °C. **B.** As in **A.**, but with *P. aeruginosa* (ATCC 27853). **C.** Endpoint hemolysis assays with defibrinated sheep blood following incubation with the indicated peptide for 18 hours at 37 °C with subsequent quantification of supernatant free hemoglobin at 414 nm. Cool colors indicate little or no release of hemoglobin. Levels throughout are the mean of three independent experiments. **D.** Alignment showing the sequence of LL-37 in comparison with shorter derivatives tested in these studies. The FF[RK] region transposed to the central activity region on which KR-12 and FK-13 are built is shown in bold with highlighting. **E.** Structure of FF-14.

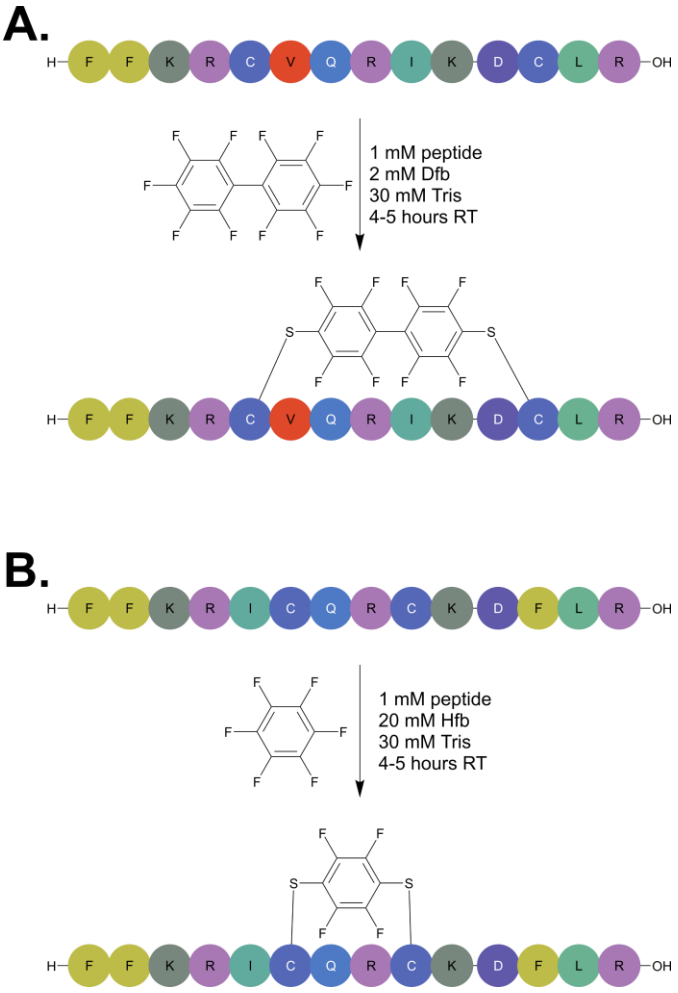
A.
H F F K R C V Q R I K D C L R OH
1 mM peptide
2 mM Dfb
30 mM Tris
4-5 hours RT
B.
H F F K R I C Q R C K D F L R OH
1 mM peptide
20 mM Hfb
30 mM Tris
4-5 hours RT

Figure 3 – General scheme for cysteine perfluoroarylation. A. Schematic showing conditions for stapling of *i,i+7* positions with decafluorobiphenyl (Dfb). **B.** Schematic showing conditions for stapling of *i,i+3* or *i,i+4* positions with hexafluorobenzene (Hfb).

A.

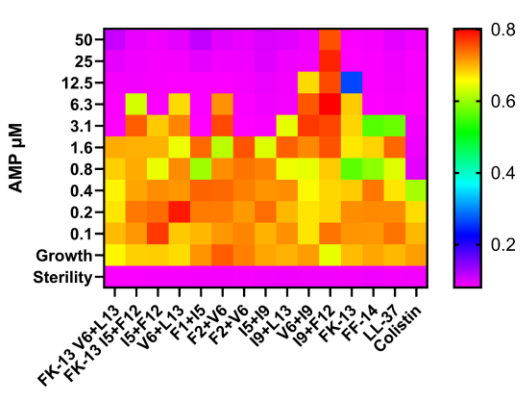

B.

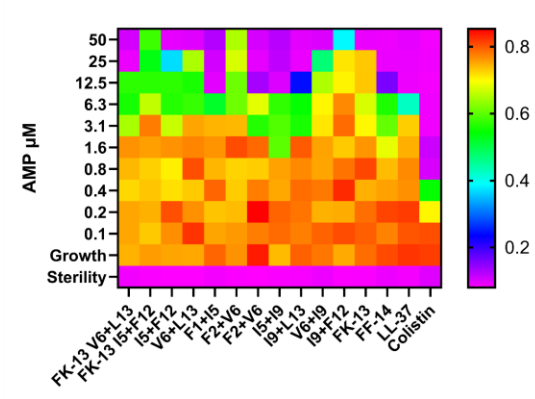

C.

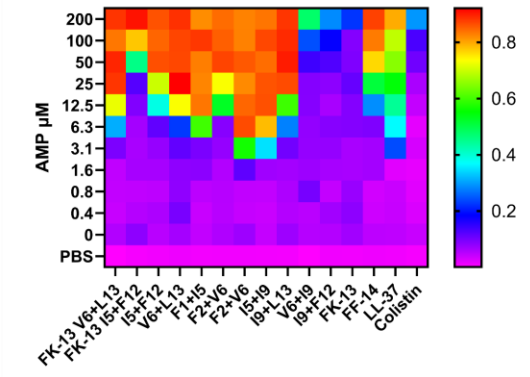

D.

FK-13 6+13	-FKRI**C**QRIKDF**C**R
FK-13 5+12	-FKR**C**VQRIKD**C**LR
I5+F12	FFKR**C**VQRIKD**C**LR
V6+L13	FFKRI**C**QRIKDF**C**R
F1+I5	**C**FKR**C**VQRIKDFLR
F2+V6	F**C**KRI**C**QRIKDFLR
F2+V6	F**C**KRI**C**QRIKDFLR
I5+I9	FFKR**C**VQR**C**KDFLR
I9+L13	FFKRIVQR**C**KDF**C**R
V6+I9	FFKRI**C**QR**C**KDFLR
I9+F12	FFKRIVQR**C**KD**C**LR
FK-13	-FKRIVQRIKDFLR
FF-14	FFKRIVQRIKDFLR

Figure 4 – Perfluoroaryl stapling yields antimicrobial activity changes that track with hemolytic activity. A. Antimicrobial susceptibility testing showing the activity of each derivative against *E. coli* (ATCC 25922). In the heatmap plate depiction, cooler colors indicate low or absent bacterial growth as detected by the OD600 measure at 18 hours of incubation at 37 °C. **B.** As in **A.**, but with *P. aeruginosa* (ATCC 27853). **C.** Endpoint hemolysis assays in which sheep RBCs in PBS were incubated with the indicated peptide for 18 hours at 37 °C. Cool colors indicate little or no release of hemoglobin as measured at 414 nm, where all levels are scaled to 100% hemolysis freeze-thaw controls. Levels throughout are the mean of three independent experiments. **D.** Alignment showing the stapled Cys residues used in each derivative.

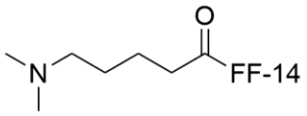

5-Dimethylamino-pentanoic Acid

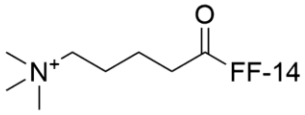

δ-Valerobetaine

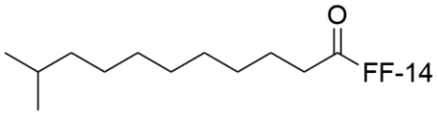

10-Methylundecanoic acid

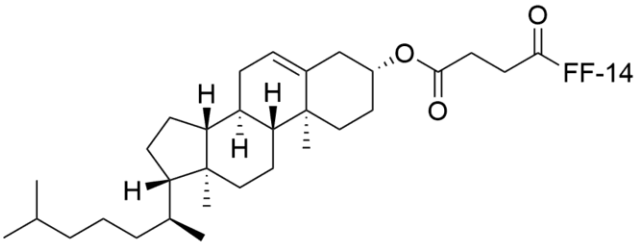

Cholesteryl Hemisuccinate

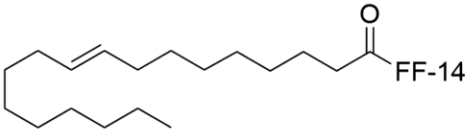

Elaidic Acid

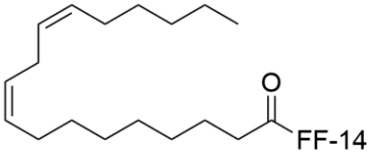

Linoleic Acid

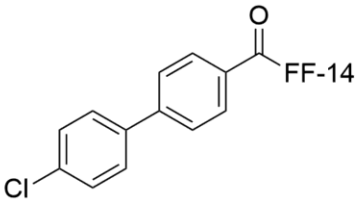

4-Chloro-biphenyl-4-carboxylic Acid

Figure 5 – N-terminal lipidation moieties appended to FF-14 and other cathelicidin derivatives. Structures of the lipid tails appended to the N-terminus of any of FF-14, LL-25, or GD-23. 5-DMA-Penta, 10-Me-Undeca, and 4-Cl-Biphenyl derive from lipoglycopeptide antibiotics, Cholesteryl is taken as a sterol representative, and Elaidic and Linoleic Acid represent longer chain mono- and poly-unsaturated tails, respectively. δ-valerobetaine is used in **Figure 7** to follow-up on the activity of 5-DMA-Penta observed in **Figure 6**. Additional N-terminal lipidation moieties in these studies are shown in **Supplementary Figure 86** with activity when appended to FK-13 shown in **Supplementary Figure 87**.

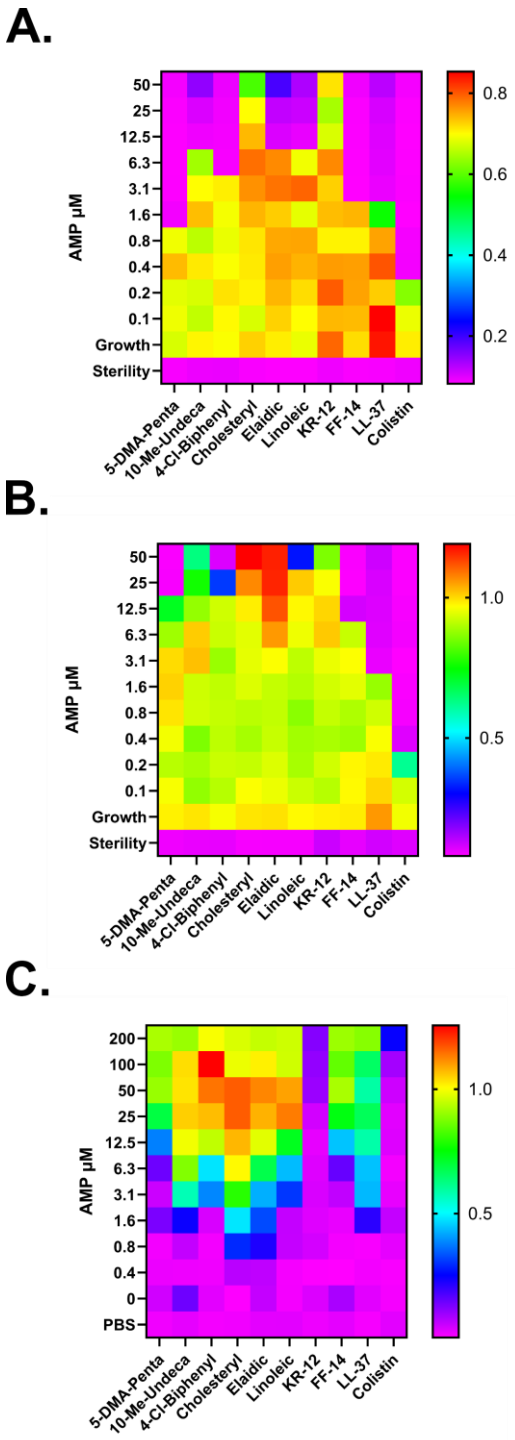
A.
AMP µM
50
25
12.5
6.3
3.1
1.6
0.8
0.4
0.2
0.1
Growth
Sterility
5-DMA-Penta
10-Me-Undeca
4-Cl-Biphenyl
Cholesteryl
Elaidic
Linoleic
KR-12
FF-14
LL-37
Colistin
0.8
0.6
0.4
0.2
B.
AMP µM
50
25
12.5
6.3
3.1
1.6
0.8
0.4
0.2
0.1
Growth
Sterility
5-DMA-Penta
10-Me-Undeca
4-Cl-Biphenyl
Cholesteryl
Elaidic
Linoleic
KR-12
FF-14
LL-37
Colistin
1.0
0.5
C.
AMP µM
200
100
50
25
12.5
6.3
3.1
1.6
0.8
0.4
0
PBS
5-DMA-Penta
10-Me-Undeca
4-Cl-Biphenyl
Cholesteryl
Elaidic
Linoleic
KR-12
FF-14
LL-37
Colistin
1.0
0.5

Figure 6 – Effects of N-terminal lipidation moieties on FF-14 activity. A. Antimicrobial susceptibility testing showing the activity of each derivative as well as a colistin control against *E. coli* (ATCC 25922). In the heatmap plate depiction, cooler colors indicate low or absent bacterial growth as detected by the OD600 measure at 18 hours of incubation at 37 °C. **B.** As in **A.**, but with *P. aeruginosa* (ATCC 27853). **C.** Hemolysis assays in which sheep RBCs in PBS were incubated with the indicated peptide for 18 hours at 37 °C with subsequent quantification of hemoglobin released into the supernatant at 414 nm. Cool colors indicate little or no release of hemoglobin, where all levels are scaled to 100% hemolysis freeze-thaw controls. Levels throughout are the mean of three independent experiments.

A.

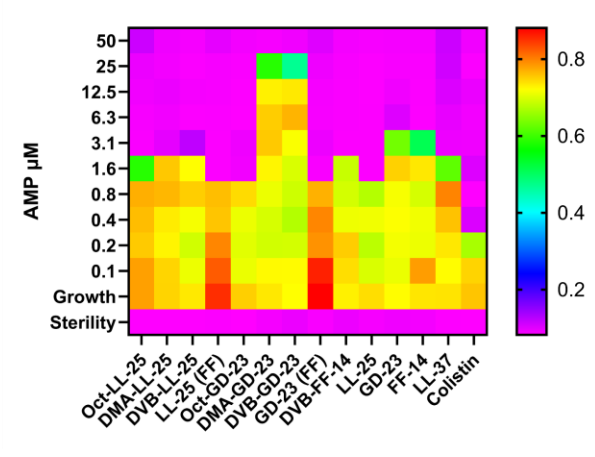
AMP µM
50
25
12.5
6.3
3.1
1.6
0.8
0.4
0.2
0.1
Growth
Sterility
Oct-LL-25
DMA-LL-25
DVB-LL-25
LL-25 (FF)
Oct-GD-23
DMA-GD-23
DVB-GD-23
GD-23 (FF)
DVB-FF-14
LL-25
GD-23
FF-14
LL-37
Colistin
0.8
0.6
0.4
0.2

B.

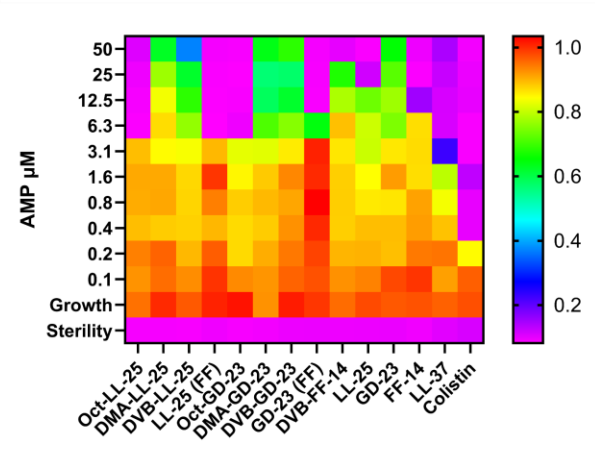
AMP µM
50
25
12.5
6.3
3.1
1.6
0.8
0.4
0.2
0.1
Growth
Sterility
Oct-LL-25
DMA-LL-25
DVB-LL-25
LL-25 (FF)
Oct-GD-23
DMA-GD-23
DVB-GD-23
GD-23 (FF)
DVB-FF-14
LL-25
GD-23
FF-14
LL-37
Colistin
1.0
0.8
0.6
0.4
0.2

C.

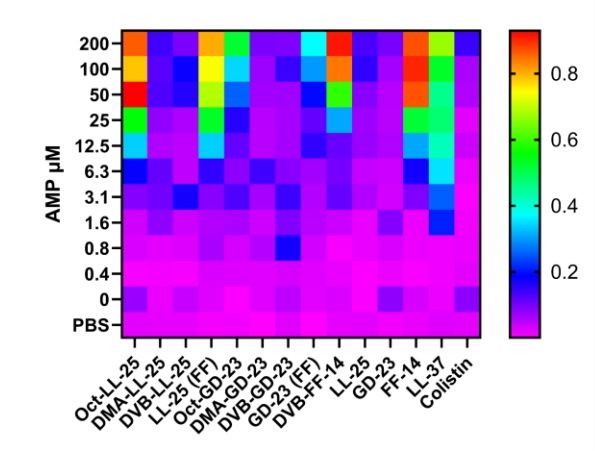
AMP µM
200
100
50
25
12.5
6.3
3.1
1.6
0.8
0.4
0
PBS
Oct-LL-25
DMA-LL-25
DVB-LL-25
LL-25 (FF)
Oct-GD-23
DMA-GD-23
DVB-GD-23
GD-23 (FF)
DVB-FF-14
LL-25
GD-23
FF-14
LL-37
Colistin
0.8
0.6
0.4
0.2

Figure 7 – Effects of selected N-terminal lipidation moieties on short cathelicidin derivatives. A. Antimicrobial susceptibility testing showing the activity of each derivative as well as a colistin control against *E. coli* (ATCC 25922). In the heatmap plate depiction, cooler colors indicate low or absent bacterial growth as detected by the OD600 measure at 18 hours of incubation at 37 °C. **B.** As in **A.**, but with *P. aeruginosa* (ATCC 27853). **C.** Hemolysis assays in which sheep RBCs in PBS were incubated with the indicated peptide for 18 hours at 37 °C with subsequent quantification of hemoglobin released into the supernatant at 414 nm. Cool colors indicate little or no release of hemoglobin, where all levels are scaled to 100% hemolysis freeze-thaw controls. Levels throughout are the mean of three independent experiments.

A.

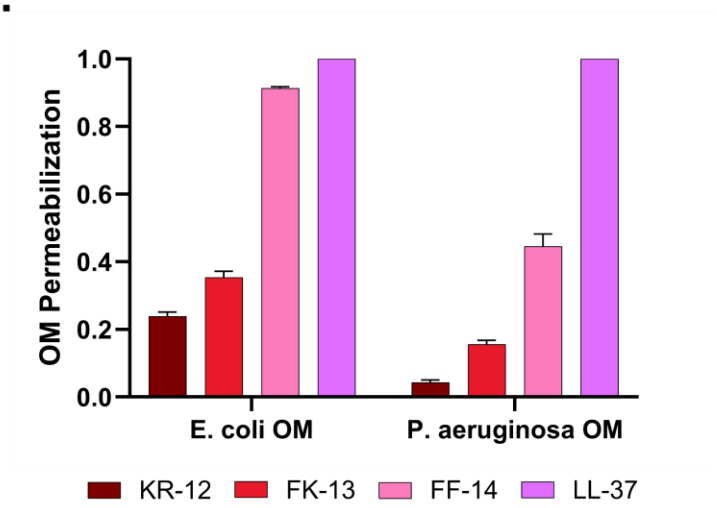

B.

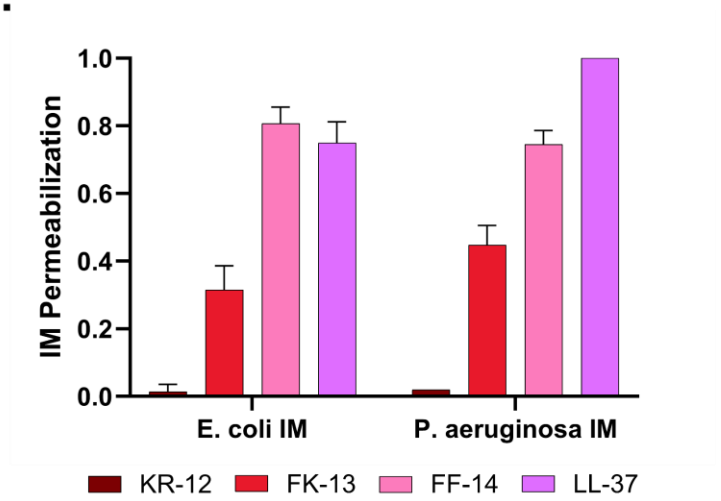

C.

		OM	IM	MIC
E. coli	KR-12	3.1	>50	>50
	FK-13	3.1	25.0	12.5
	FF-14	1.6	12.5	3.1
	LL-37	0.8	1.6	3.1
P. aeruginosa	KR-12	>50	>50	>50
	FK-13	50.0	25.0	50.0
	FF-14	6.3	6.3	6.3
	LL-37	0.8	0.8	3.1

Figure 8 – Relative outer and inner membrane permeabilization of short cathelicidin derivatives. Dual membrane permeabilization assays were completed by incubating *E. coli* (ATCC 25922) or *P. aeruginosa* (ATCC 27853) in the presence of N-phenyl-naphthylamine as a marker of outer membrane permeabilization (**A**) and propidium iodide as a marker of inner membrane permeabilization (**B**) in the presence of varying concentrations of each indicated peptide. Permeabilization was then quantified over the course of 240 minutes relative to LL-37. The single-point permeabilization index presented represents the product of the peak permeabilization signal relative to LL-37 multiplied by the proportion of the 240-minute incubation required to surpass 80% of the maximum signal observed for each peptide. Full kinetic curves associated with each condition are shown in **Figures S151-154. C.** Comparison of the lower limits of detection of permeabilization set to 10% of LL-37 peak relative to MIC.